AMULET

Growing

Early-career

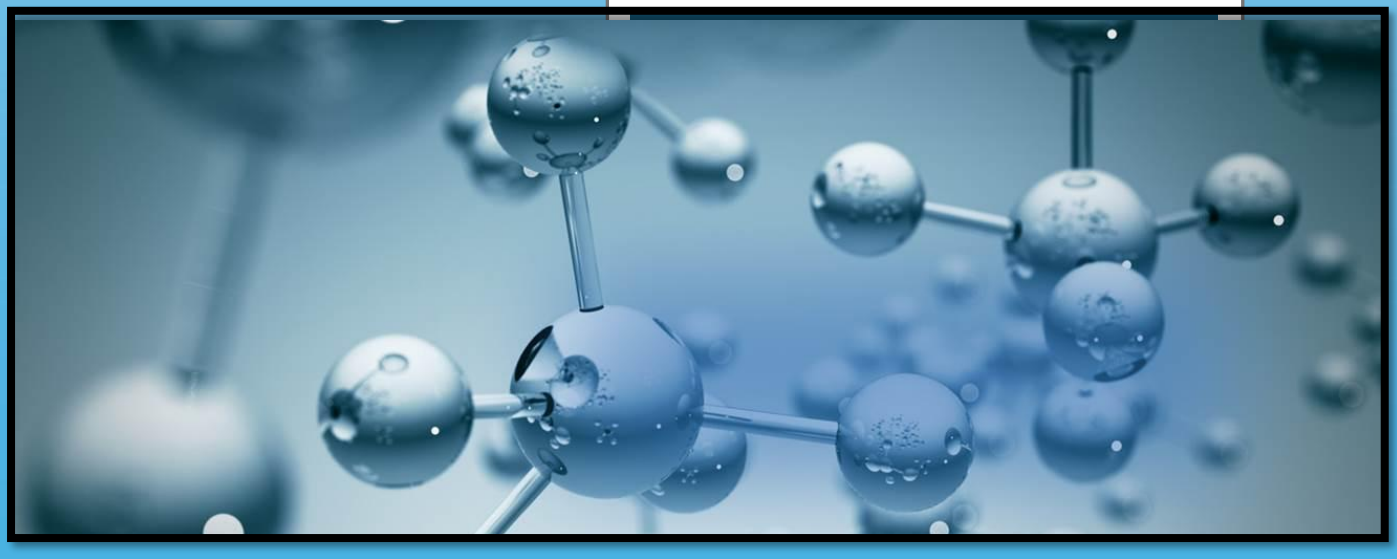
MindS

May 2026

Task Forum 2026

PROCEEDING PAPERS

AMULET



TASK FORUM 2026

AMULET Growing Early-career MindS workshop

May 7, 2026
Prague, Czech Republic

This publication is intended for conference participants and members of the organizing organizations. The authors are fully responsible for the content of their texts. The publication has not undergone any language editing.

Use of this work is governed by the Creative Commons Attribution License 4.0 (https://creativecommons.org/licenses/by/4.0/), which permits unrestricted use, distribution, and copying of the work in any medium, provided the work title, authors, source, and license are properly credited.

DOI: 10.66951/TLMZ8719
https://doi.org/10.66951/TLMZ8719
https://creativecommons.org/licenses/by/4.0/

Title:	**Task Forum 2026**
Publisher:	Heyrovsky Institute od the CAS, Dolejškova 2155/3, 182 00 Praha 8
Editors:	Martin Kalbáč, Zuzana Sochorová, Klaudie Soukupová
Authors:	*Collective of authors* Oleksandr Volochanskyi, Heyrovský Institute of the CAS Olha Zin, Heyrovský Institute of the CAS Jan Kozisek, Charles University Viktorie Neubertová, University of Jan Evangelista Purkyně Rahul Kesarwani, Charles University Štefan Hricov, Charles University Eva Štěpanovská, Institute of Nuclear Physics of the CAS Martin Lamač, Heyrovský Institute of the CAS Michal Trčka, Heyrovský Institute of the CAS
Language:	English
Number of pages:	58
Print run:	electronic version only
Issued:	May 2026
Edition:	1st
ISBN:	978-80-87351-74-1

Co-funded by the European Union
Ministry of Education, Youth and Sports of the Czech Republic
AMULET



On May 7, 2026, the one-day student conference Task Forum 2026, organized by the AMULET project, took place at the Institute of Physics of the Czech Academy of Sciences. The event brought together around 50 participants from various fields including materials research, physics, chemistry, biomedicine, and nanotechnology. The conference primarily provided space for PhD students and postdoctoral researchers to present their current research projects and discuss them with colleagues across disciplines.

The AMULET project focuses on advanced engineering of multiscale materials — from designing structures at the sub-nanometer level to integrating them into functional devices for applications in electronics, medicine, and environmental technologies. The research combines state-of-the-art experimental and theoretical approaches and also addresses the societal and economic impacts of emerging technologies. Interdisciplinary collaboration and knowledge sharing are among the project's core principles, which were clearly reflected in the conference programme.

Students Presented Results Across All Work Packages

Students from all five research areas of the AMULET project presented their work — ranging from the development of multiscale materials and biointerfacing to chemical and biological sensors, catalysis, and new electronic and optoelectronic devices. The programme included topics such as biosensors, photocatalysis, subnanometer catalysis, hybrid antimicrobial platforms, bioimaging, and resilient nanoelectronics. Thanks to the broad thematic scope, discussions often led to unexpected connections and new ideas.

Space for New Collaborations

The conference was also attended by senior scientists who supervise student projects within AMULET and share their experience from international research with the younger generation. Among them were Martin Kalbáč, Jana Kalbáčová Vejpravová, Anna Macková, Zdeňka Kolská, Hana Tarábková, Otakar Frank, and others. Their presence highlighted the importance of intergenerational collaboration in science, where experience meets the fresh ideas and energy of early-career researchers.

The conference also emphasized the crucial role of supporting young scientists in contemporary research. PhD students and early-career researchers are often those bringing new perspectives, the courage to experiment, and the ability to connect disciplines that previously had little interaction. Events like this provide them not only with an opportunity to present their own results, but also to gain experience in scientific discussion, establish international contacts, and explore future collaborations.



PROCEEDING PAPERS

Prague
May 7, 2026

Co-funded by the European Union
Ministry of Education, Youth and Sports of the Czech Republic
AMULET

Table of Contents

BROADBAND PHOTO RESPONSE OF GRAPHENE/COFE2O4 NANOPARTICLE PHOTODETECTORS UNDER AC AND DC DRIVING CONDITIONS 4

VISIBLE-LIGHT-ACTIVE TITANIUM DIOXIDE PHOTOCATALYSTS PREPARED BY A MECHANOCHEMICAL APPROACH 9

INVESTIGATION OF PLASMON-DRIVEN REACTIONS OF 4-MERCAPTOPHENYLBORONIC ACID ON SILVER NANOPARTICLES: A SERS STUDY 14

DEVELOPMENT OF HYBRID ANTIMICROBIAL PLATFORMS VIA COORDINATION CHEMISTRY 19

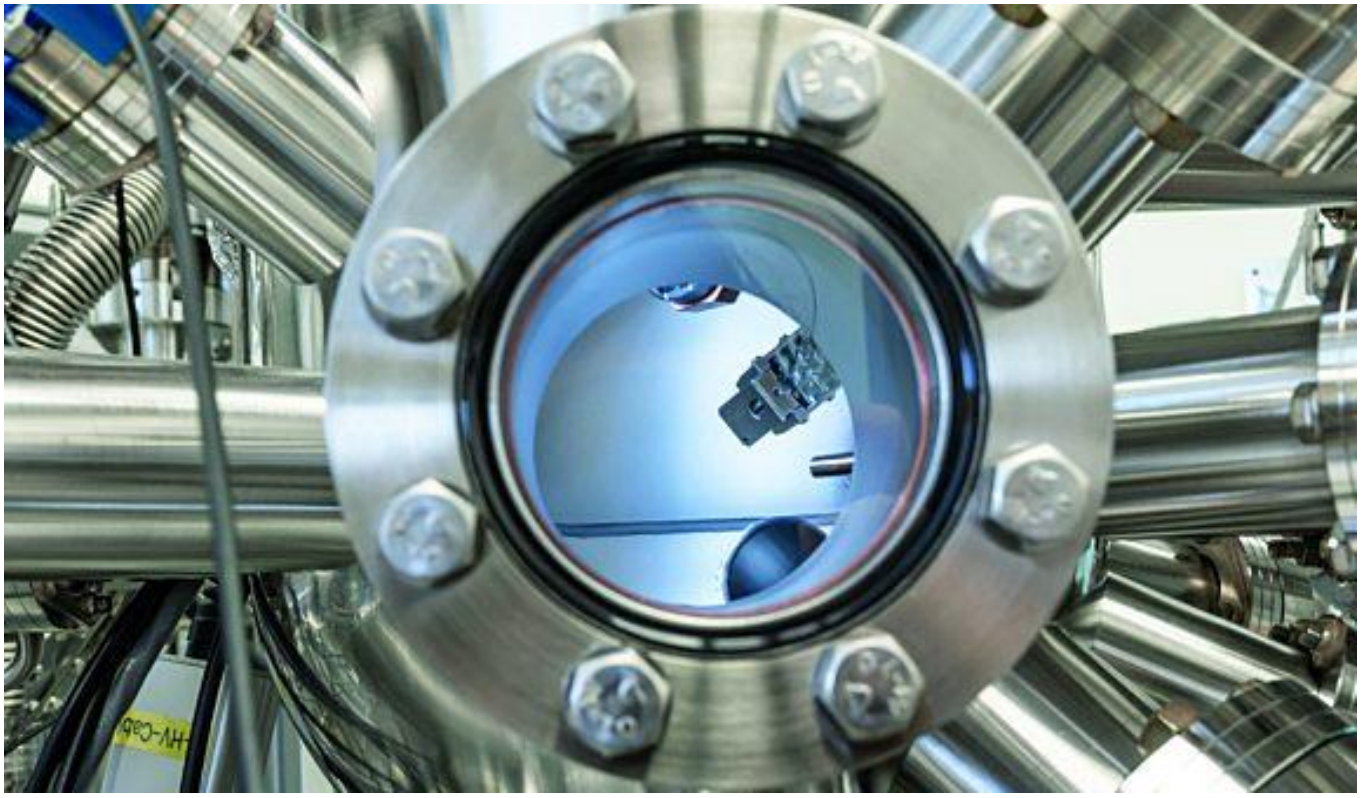
TRANSITION METAL DICHALCOGENIDE NANOSCROLLS: STRUCTURE, PROPERTIES AND EMERGING APPLICATIONS . 25

HYDROPHOBIC ZNFE2O4 MAGNETIC NANOPARTICLES WITH WELL-DEFINED SUPERBALL MORPHOLOGY AND ROOM-TEMPERATURE SUPERPARAMAGNETISM 31

ION-BEAM ENGINEERING AS A PHYSICAL STRATEGY FOR ELECTROCHEMICAL MATERIALS DESIGN 37

ACTIVATED BORANE MATERIALS FOR HETEROGENEOUS CATALYTIC DEHALOGENATION 42

NEGOTIATING OPEN SCIENCE: SOCIOLOGICAL PERSPECTIVES FROM THE AMULET PROJECT 45



Co-funded by the European Union

Ministry of Education, Youth and Sports of the Czech Republic

AMULET

BROADBAND PHOTO RESPONSE OF GRAPHENE/COFE2O4 NANOPARTICLE PHOTODETECTORS UNDER AC AND DC DRIVING CONDITIONS

DOI: 10.66951/HTZA1753; https://doi.org/10.66951/HTZA1753

Oleksandr Volochanskyi, oleksandr.volochanskyi@heu.cas.cz
Heyrovský Institute, Czech Academy of Sciences, Dolejškova 2155/3, 182 23 Prague, Czech Republic

Department of Physical Chemistry, University of Chemistry and Technology Prague, Technická 5, 166 28 Prag ue, Czech Republic

Golam Haider, g.haider@ifw-dresden.de
Heyrovský Institute, Czech Academy of Sciences, Dolejškova 2155/3, 182 23 Prague, Czech Republic

Martin Mergl, martin.mergl@heu.cas.cz
Heyrovský Institute, Czech Academy of Sciences, Dolejškova 2155/3, 182 23 Prague, Czech Republic

Stefania Sandoval Rojano, ssandoval@icmab.es
Heyrovský Institute, Czech Academy of Sciences, Dolejškova 2155/3, 182 23 Prague, Czech Republic

Martin Kalbáč, martin.kalbac@heu.cas.cz
Heyrovský Institute, Czech Academy of Sciences, Dolejškova 2155/3, 182 23 Prague, Czech Republic

Abstract

For hybrid photodetectors with electrically complex interfaces, the choice of measurement scheme determines the quality and meaning of the obtained photoresponse. Hybrid graphene photodetectors combine the high carrier mobility and broadband optical response of graphene with light-sensitive materials that modify the electrical properties of the graphene channel, yet their response is commonly evaluated under a constant source–drain bias that also records transient current changes developing during continuous bias and illumination. Here, we compare direct current (DC) and alternating current (AC) measurement scheme of graphene devices functionalized with oleic-acid-capped $CoFe_2O_4$ nanoparticles. Under a constant 2 V bias, illumination produces a measurable broadband response together with pronounced current transients after light switching. In contrast, a 100 kHz sinusoidal bias with small amplitude produces stable and reproducible illumination-dependent AC current. Frequency-resolved impedance measurements show that the device evolves from predominantly resistive behavior at low frequency to a mixed resistive–reactive response near 100 kHz, with illumination modifying both components of the complex admittance. This frequency-selective measurement enables clear detection across 500–1100 nm, including weak response at 1100 nm that is difficult to resolve reliably in the DC traces. These results show that AC driving conditions can improve the practical detectability of weak optical signals in interface-dominated hybrid photodetectors.

1 Introduction

Graphene provides a high-mobility transport channel with optical sensitivity over a broad spectral range, but its weak absorption limits the photoresponse of simple graphene devices [1,2]. Hybrid architectures address this by coupling graphene to an additional light-sensitive material whose photoexcitation modifies the carrier density, conductivity, or electrostatic environment of the graphene channel [1,3]. In colloidal nanoparticle systems, the interface enabling this coupling can also impede charge transport. Long-chain surface ligands provide colloidal stability but act as barriers to electronic coupling and carrier transport in nanocrystal solids [4,5]. Oleic acid is widely used in the synthesis and stabilization of $CoFe_2O_4$ nanoparticles and binds directly to the ferrite surface [6]. Consequently, an oleic-acid-capped $CoFe_2O_4$/graphene interface contains an electronically resistive organic layer in the potential charge-transfer pathway. The extent to which this interface contributes resistive or capacitive components to the device response must therefore be determined experimentally.

Hybrid graphene photodetectors are commonly characterized under a constant DC source–drain bias, where illumination-induced changes in device conductance are recorded directly as changes in current [1,3], $I_{\mathrm{ph,DC}} = I_{\mathrm{light}} - I_{\mathrm{dark}}$. Time-dependent measurements performed under such conditions collect both the steady illuminated–dark current difference and transient current evolution following changes in illumination [7]. In hybrid devices with interface-limited charge transport, such transients can arise from charge accumulation and delayed release at the sensitizer/graphene interface and may obscure weak optical signals when their magnitude becomes comparable to the steady photoresponse. AC driving conditions provide a complementary measurement scheme. A sinusoidal voltage periodically reverses the source–drain electric field, and frequency-selective detection scheme measures the electrical response at the applied frequency. Contributions that vary much more slowly than this driving conditions appear less directly in the measured AC-driven measurements. At higher frequencies where the device exhibits a non-negligible reactive component, the measured AC current depends on the full complex admittance, $Y = G + jB$. Frequency-resolved impedance measurements are therefore required to interpret the AC photoresponse [8].

Here, we compare DC and AC electrical test schemes of graphene devices functionalized with oleic-acid-capped $CoFe_2O_4$ nanoparticles. Frequency-dependent impedance measurements are combined with time-dependent and wavelength-dependent optical measurements to establish how the electrical AC/DC test scheme affects the measured response. The purpose of this study is to determine whether frequency-selective AC readout can improve the stability and practical detectability of the broadband photoresponse in an interface-dominated graphene/nanoparticle photodetector.

2 Main Section

Oleic-acid-capped $CoFe_2O_4$ nanoparticles were synthesized following the procedure reported in Ref. [9] and deposited onto the graphene devices by spin coating. The graphene/$CoFe_2O_4$ nanoparticle device and representative DC and AC responses are shown in **Figure 1**. Under DC operation, a constant source–drain bias of 2 V produces a measurable current change when the illumination is switched on, together with pronounced transient features at the illumination transitions (**Figure 1c**). Similar transients are observed when the illumination is removed. Comparable transients were absent in pristine graphene devices measured before $CoFe_2O_4$ deposition, identifying the nanoparticle layer or the newly formed nanoparticle/graphene interface as their likely origin. The oleic-acid ligand shell provides a plausible contribution because long-chain aliphatic ligands impede electronic coupling and charge transport in colloidal nanoparticle systems [4–6], while surface modification or partial decomposition of the nanoparticles may introduce additional localized states. Both effects can promote charge

accumulation and delayed release at the interface, consistent with the transient current spikes observed under DC bias.

For AC measurements, a sinusoidal source–drain voltage of V_{pp} = 50 mV was applied. At 100 kHz the electrical period is 10 µs, and the polarity of the applied field reverses every 5 µs (**Figure 1B**). The measured I_{AC} represents the RMS current at the applied test frequency. Under these experimental conditions, illumination instead produces stable changes in the measured AC current, ΔI_{AC}, without the pronounced switching transients observed under DC bias (**Figure 1D**).

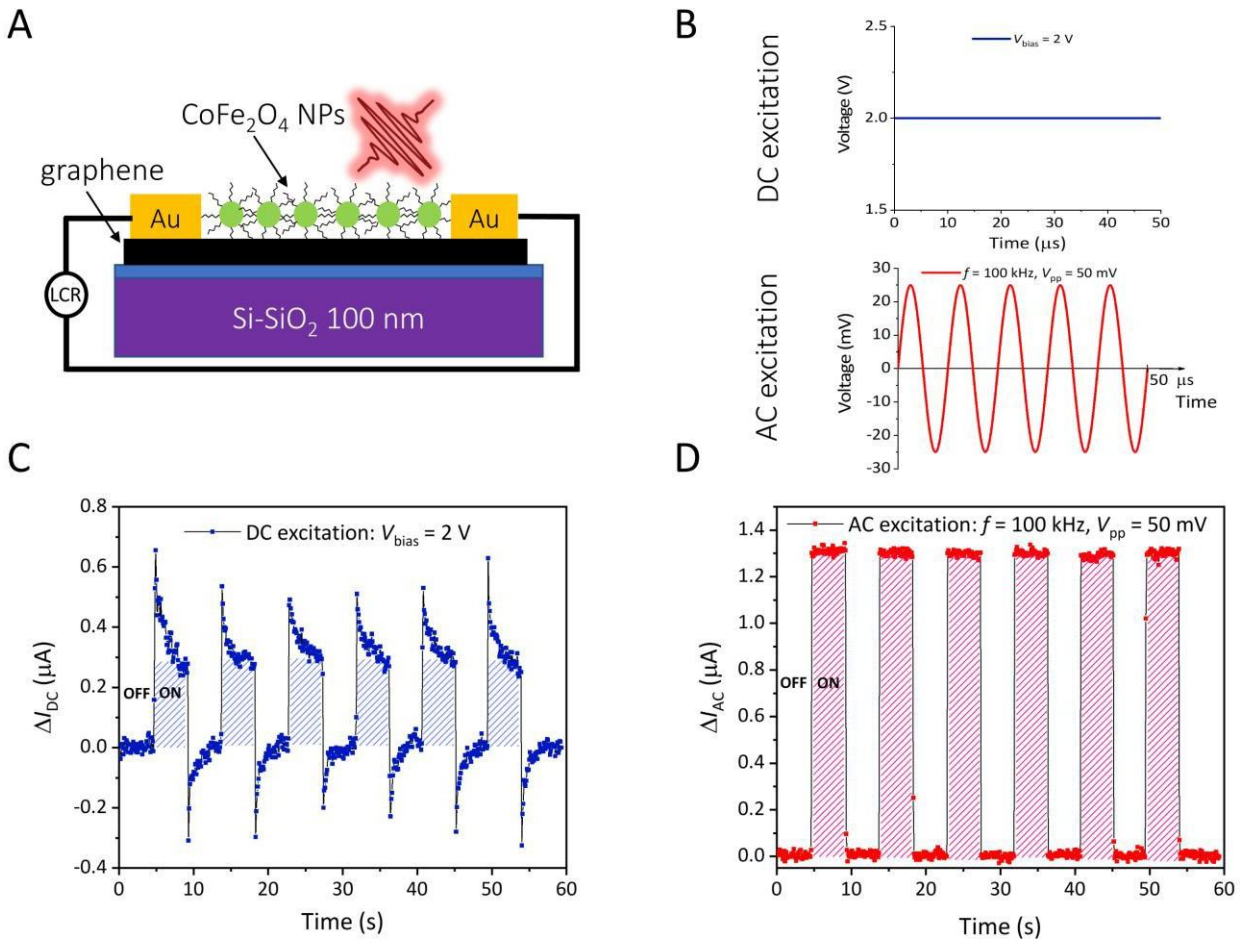


Figure 1. Device architecture and comparison of DC and AC electrical response. (A) Schematic of the graphene device functionalized with oleic-acid-capped $CoFe_2O_4$ nanoparticles and contacted by Cr/Au electrodes on a Si-SiO_2 substrate. Electrical measurements were performed using an LCR meter. (B) Applied voltage in the two measurement modes: a constant bias of V_{bias} = 2 V for DC measurements and a sinusoidal voltage at f = 100 kHz and V_{pp} = 50 mV for AC measurements. (C) Representative DC photoresponse under repeated illumination, showing pronounced transient current spikes after switching the light on and off, followed by relaxation toward the illuminated or dark level. (D) Corresponding AC photoresponse measured at 100 kHz, showing stable and reproducible light-on and light-off levels with strongly suppressed transient features. Hatched regions indicate illumination ON. AC and DC data were collected using Hioki Im3533-01 LCR meter.

Frequency-resolved impedance measurements were used to determine the electrical character of the AC response (**Figure 2A**). The complex impedance $Z = R_S + jX$ is predominantly resistive at low frequency, where reactance X approaches zero. With increasing frequency, the negative reactance becomes substantial and is comparable in magnitude to R_S near the 100 kHz operating condition, demonstrating a mixed resistive–capacitive response. To isolate the illumination-induced contribution, the impedance was converted to admittance, $Y = G + jB = 1/Z$, and the corresponding dark levels were subtracted (**Figure 2B**). Both conductance ΔG, i.e. the in-phase/dissipative contribution, and susceptance ΔB, i.e. the reactive contribution, increase with frequency and optical power density,

showing that illumination modifies both the conductive and reactive components of the device response. Thus, the measured AC photoresponse represents a light-induced change in complex admittance, $I_{AC} = V_{AC,rms}|Y|$. The increasing AC photoresponse with frequency is therefore associated with the frequency-dependent light-induced modulation of the complex admittance, with contributions from both conductance and susceptance.

The practical advantage of AC regime is most apparent in the wavelength-dependent measurements (**Figure 2C, D**). Both DC and AC measurements detect a broadband response from 500 to 1100 nm. Under a constant DC bias, however, illumination switching is accompanied by pronounced current transients and relaxation, which increasingly complicates extraction of the weak response at longer wavelengths. At 100 kHz and V_{pp} = 50 mV, stable and reproducible AC current changes are obtained across the complete spectral range, allowing the response at 1100 nm to remain clearly resolved. Frequency- selective AC measurement therefore improves the practical visibility of weak optical signals in this interface-dominated device, while detailed impedance analysis is required to establish the electrical meaning of the measured AC response.

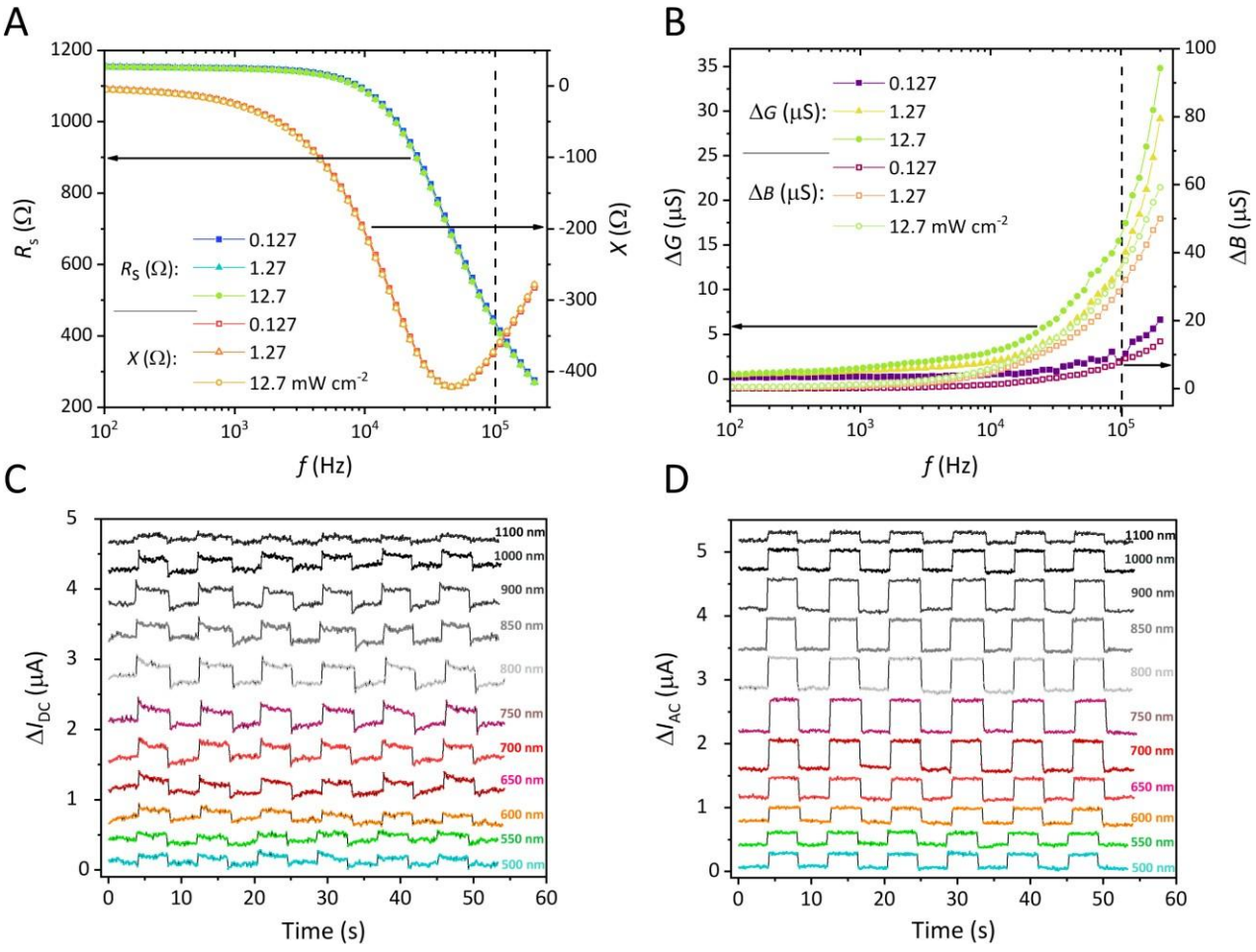


Figure 2. Frequency-dependent electrical response and wavelength-dependent response under DC and AC conditions. (A) Series-equivalent resistance R_s and reactance X of the graphene/$CoFe_2O_4$ nanoparticle device as a function of frequency under 700 nm illumination. The increasingly negative reactance indicates the development of a capacitive contribution with increasing frequency. The dashed line marks 100 kHz, used for the AC photoresponse measurements. (B) Light-induced changes in conductance, $\Delta G = G_{light} - G_{dark}$, and susceptance, $\Delta B = B_{light} - B_{dark}$, calculated from the complex impedance at the same optical powers. Both components increase with frequency and optical power, demonstrating that illumination modifies both the conductive and reactive response of the device. (C,D) Wavelength-dependent photoresponse measured from 500 to 1100 nm under (C) a constant 2 V DC bias and (D) a 100 kHz, V_{pp} = 50 mV of AC driving conditions. Traces are vertically offset for clarity. The AC readout provides reproducible light-on and light-off levels throughout the measured spectral range, including the weak response at 1100 nm. AC and DC data were collected using Hioki Im3533-01 LCR meter.

3 Conclusions

DC and AC measurements reveal complementary aspects of the photoresponse in graphene/$CoFe_2O_4$ nanoparticle devices. Continuous DC bias exposes pronounced transient behavior and is consistent with interface-limited charge redistribution. AC measurements at 100 kHz provide a substantially more stable response, enabling weak broadband signals to be resolved reproducibly up to 1100 nm. Frequency-dependent impedance measurements show that illumination modifies both conductance and susceptance at the selected AC frequency, confirming contributions from both conductive and reactive components. These results demonstrate that the electrical test scheme is an important design parameter for hybrid photodetectors with electrically complex interfaces.

4 Acknowledgement

This work has been funded by a grant from the Programme Johannes Amos Comenius under the Ministry of Education, Youth and Sports of the Czech Republic CZ.02.01.01/00/22_008/0004558 Advanced MUltiscaLe materials for key EnablingTechnologies.

5 References

[1] F. H. L. Koppens, T. Mueller, Ph. Avouris, A. C. Ferrari, M. S. Vitiello, M. Polini, *Nat. Nanotechnol.* **9** (2014) 780–793. DOI: 10.1038/nnano.2014.215.

[2] R. R. Nair, P. Blake, A. N. Grigorenko, *et al.*, *Sci.* **320** (2008) 1308. DOI: 10.1126/science.1156965.

[3] G. Konstantatos, M. Badioli, L. Gaudreau, *et al.*, *Nat. Nanotechnol.* **7** (2012) 363–368. DOI: 10.1038/nnano.2012.60.

[4] D. V. Talapin, J.-S. Lee, M. V. Kovalenko, E. V. Shevchenko, *Chem. Rev.* **110** (2010) 389– 458. DOI: 10.1021/cr900137k.

[5] X. Liang, S. Bai, X. Wang, *et al.*, *Chem. Soc. Rev.* **46** (2017) 1730–1759. DOI: 10.1039/C6CS00122J.

[6] S. M. Ansari, B. B. Sinha, D. Phase, *et al.*, *ACS Appl. Nano Mater.* **2** (2019) 1828–1843. DOI: 10.1021/acsanm.8b02009.

[7] C. O. Kim, S. W. Hwang, S. Kim, *et al.*, *Sci. Rep.* **4** (2014) 5603. DOI: 10.1038/srep05603.

[8] E. von Hauff, *J. Phys. Chem. C* **123** (2019) 11329–11346. DOI: 10.1021/acs.jpcc.9b00892.

[9] S. A. Kadam, S. Sandoval, Z. Bastl, *et al.*, *ACS Catal.* **13** (2023) 13484–13505. DOI: 10.1021/acscatal.3c02592.

VISIBLE-LIGHT-ACTIVE TITANIUM DIOXIDE PHOTOCATALYSTS PREPARED BY A MECHANOCHEMICAL APPROACH

DOI: 10.66951/YLMT8345; https://doi.org/10.66951/YLMT8345

Olha Zin, olha.zin@jh-inst.cas.cz
J. Heyrovský Institute of Physical Chemistry of the CAS, v.v.i., Prague, Czech Republic

Volodymyr Sydorchuk, Libor Brabec, Jiří Rathouský, Lenka Belháčová, Joanna Elżbieta Olszówka
J. Heyrovský Institute of Physical Chemistry of the CAS, v.v.i., Prague, Czech Republic

Abstract

The development of photocatalysts active under visible-light irradiation remains a major challenge due to the limited spectral response of titanium dioxide (TiO_2). In this work, a simple mechanochemical approach based on high-energy ball milling was employed to prepare visible-light-active TiO_2 photocatalysts from both synthesized and commercial anatase and rutile powders. The influence of milling conditions on phase composition, surface properties, optical characteristics, and photocatalytic performance was systematically investigated. Ball milling induced partial transformation of anatase to rutile, the formation of anatase/rutile interfaces, and the generation of oxygen vacancies. These structural modifications enhanced visible-light absorption and led to band-gap narrowing. Photocatalytic activity was evaluated through the degradation of 4-chlorophenol under blue-light irradiation. The milled anatase samples exhibited significantly higher activity than both the pristine materials and the commercial Evonik P25 reference photocatalyst. The highest degradation efficiency was achieved with ball-milled sol-gel-derived anatase, reaching up to 65% degradation after 5 h of irradiation. The prepared materials also performed well when deposited as stable coatings on glass substrates.

1 Introduction

Semiconductor photocatalysis has attracted considerable attention as an environmentally friendly technology for water purification, air treatment, and self-cleaning surfaces [1–3]. Titanium dioxide is one of the most extensively studied photocatalysts owing to its chemical stability, low toxicity, abundance, and low cost. However, its practical application is limited by its wide band gap, which restricts photoactivation primarily to ultraviolet radiation [2,3].

Numerous strategies have been explored to extend the photoresponse of TiO_2 into the visible-light region, including doping with metal and non-metal elements, coupling with narrow-band-gap semiconductors, and surface modification [2,3]. Although these approaches have shown promising results, many suffer from drawbacks such as poor long-term stability, complex synthesis procedures, or high production costs.

Mechanochemical treatment offers an attractive alternative, as it can modify the crystal structure and defect concentration without introducing foreign elements [3]. The aim of this work was to develop visible-light-active TiO_2 photocatalysts using a simple ball-milling approach and to investigate the relationship between their physicochemical properties and photocatalytic performance.

2 Work performed / Main Section (it could be several sections)

2.1 Preparation of photocatalysts

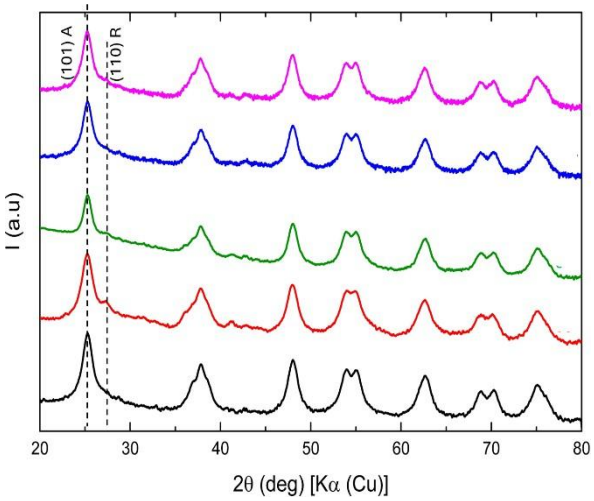


Titanium dioxide samples (**Figure 1.**) were prepared from different precursors. Anatase was synthesized by precipitating titanium hydroxide from $TiCl_4$, followed by calcination at 500 °C, while rutile was obtained by calcination at 900 °C. Additionally, anatase samples were produced via a sol–gel route using titanium butoxide. For comparison, commercial anatase TiO_2 was also included.

Figure 1. Illustration of TiO2 milled sample.

The powders were subjected to high-energy ball milling in air at rotational speeds of 300-600 rpm. The milling process required less than one hour and produced significant structural modifications.

2.2 Physicochemical characterization



X-ray diffraction analysis revealed that milling of the precipitated anatase (**Figure 2.**) induced partial transformation into rutile, resulting in anatase/rutile mixtures containing approximately 6–10 % rutile. In contrast, milling of commercial anatase and rutile led to the formation of small amounts of the high-pressure TiO_2-II (srilankite) phase [4].

Figure 2. XRD patterns of precipitated anatase.

Nitrogen adsorption measurements showed that the precipitated anatase retained a high specific surface area after milling, ranging from 84 to 105 $m^2 g^{-1}$. Such high surface areas are advantageous for photocatalytic processes because they provide more active adsorption sites.

UV–Vis spectroscopy confirmed enhanced visible-light absorption following mechanochemical treatment [4]. The absorption edge shifted from 382 nm for the initial anatase to 401 nm for the sample milled at 450 rpm. Correspondingly, the band gap decreased from approximately 3.25 eV to about 3.02–3.09 eV. Electron paramagnetic resonance measurements further verified the formation of oxygen vacancies and other structural defects generated during milling [4].

2.3 Photocatalytic activity

Photocatalytic degradation experiments were carried out using an aqueous solution of 4-chlorophenol (4-CP) with an initial concentration of 1×10^{-4} M. The reaction was performed in a 25 mL quartz cuvette equipped with an external cooling system that maintained the temperature at 20 °C. Irradiation was provided by three blue LEDs emitting at 440–445 nm, resulting in an irradiance of 20 mW cm^{-2} inside the cuvette, as measured with an ILT2400 radiometer (International Light Technologies) [5] (**Figure 3.**).

The initially precipitated anatase exhibited only 17% degradation after 5 h, whereas the milled samples showed markedly higher activity. The sample milled at 450 rpm achieved 59 % degradation, and the sol-gel-derived anatase milled at 600 rpm reached 65 % degradation [4].

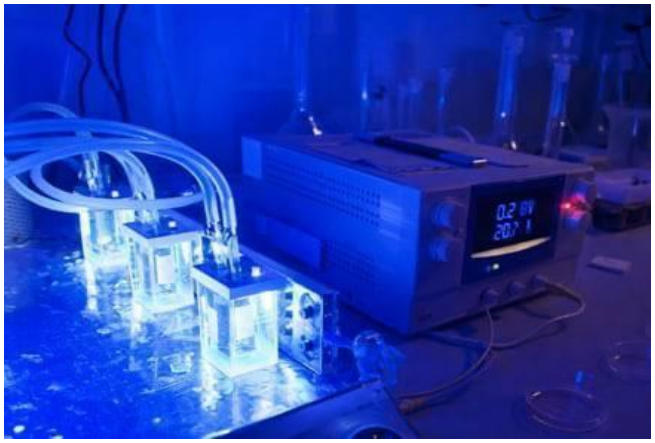


Figure 3. Experimental setup used for photocatalytic degradation of 4-chlorophenol under blue LED irradiation.

The degradation rate of constants increased substantially after mechanochemical treatment and exceeded those obtained for the commercial Evonik P25 photocatalyst (**Figure 4.**). The improved activity can be attributed to several synergistic effects, including the formation of anatase/rutile homojunctions, increased concentration of oxygen vacancies, enhanced visible-light absorption, and preservation of a high specific surface area [3,4].

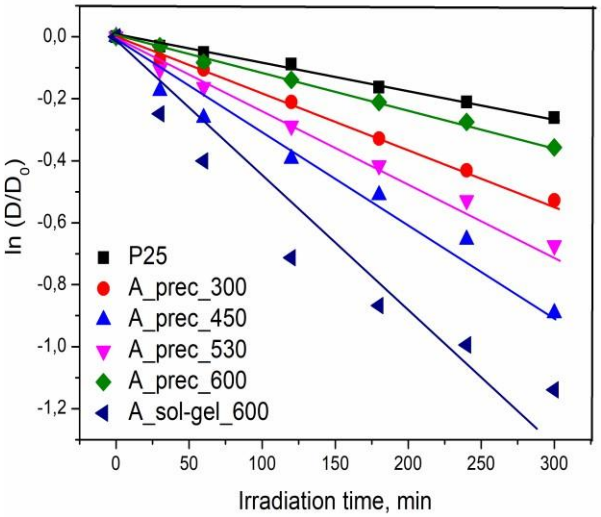


Figure 4. Kinetic curves of 4-chlorophenol degradation under blue-light irradiation for TiO_2 photocatalysts prepared by high-energy ball milling in powder form.

The photocatalytic degradation pathway was further investigated by identifying intermediate products, including benzoquinone, hydroquinone, and chlorocatechol [4]. Significant mineralization of organic compounds was confirmed by total organic carbon measurements.

2.4 Photocatalytic coatings

For practical applications, selected photocatalysts were deposited onto glass substrates. The resulting coatings exhibited photocatalytic activity (**Figure 5.**) comparable to that of the powder samples while maintaining good stability and reusability [4]. These findings highlight the potential of the developed materials for use in self-cleaning surfaces and environmental remediation technologies.

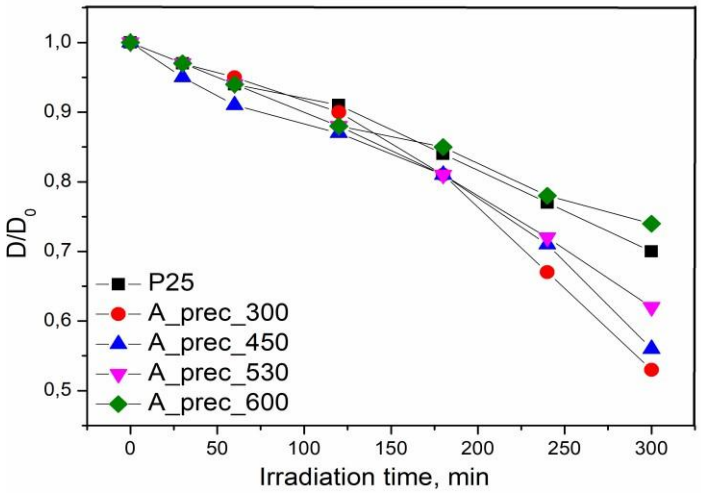


Figure 5. Kinetic curves of 4-chlorophenol degradation under blue-light irradiation for TiO_2 photocatalysts prepared by high-energy ball milling as layers.

3 Conclusions / Further Research / Summary / Discussion

A simple mechanochemical method based on high-energy ball milling was successfully employed to prepare TiO_2 photocatalysts active under visible light. Ball milling induced partial transformation of anatase to rutile, generated oxygen vacancies, and enhanced visible-light absorption. These structural modifications led to a significant improvement in photocatalytic activity during the degradation of 4-chlorophenol under blue-light irradiation.

Among the investigated materials, the ball-milled sol-gel-derived anatase exhibited the highest photocatalytic performance, surpassing both the initial TiO_2 powders and the commercial Evonik P25 reference. The prepared photocatalysts also demonstrated promising performance when applied as stable coatings on glass substrates.

Overall, the proposed approach provides a rapid, scalable, and economically viable route for producing advanced TiO_2-based photocatalysts for visible-light-driven environmental applications.

4 Acknowledgement

This work was supported by the Johannes Amos Comenius Program of the Ministry of Education, Youth and Sports of the Czech Republic, grant no. 02.01.01/00/22_008/0004558 Advanced Multiscale Materials for Key Enabling Technologies.

5 References

[1] Fujishima, A.; Honda, K. Electrochemical Photolysis of Water at a Semiconductor Electrode. Nature, 1972, 238, 37–38.

[2] Chen, X.; Mao, S.S. Titanium Dioxide Nanomaterials: Synthesis, Properties, Modifications and Applications. Chemical Reviews, 2007, 107, 2891–2959.

[3] Schneider, J.; Matsuoka, M.; Takeuchi, M.; Zhang, J.; Horiuchi, Y.; Anpo, M.; Bahnemann, D.W. Understanding TiO_2 Photocatalysis: Mechanisms and Materials. Chemical Reviews, 2014, 114, 9919– 9986.

[4] Zin, O.; Sydorchuk, V.; Brabec, L.; Rathouský, J.; Belháčová, L.; Olszówka, J.E. Development of Visible-Light-Active Titanium Oxide Photocatalysts Prepared by Mechanochemical Approach. AMULET GEM Task Forum, 2026.

[5] L. Brabec, Supported g C3N4/WO3 mixed layers for photocatalytic water remediation, Chemical Papers, 78 (2024) 8749–8757.

INVESTIGATION OF PLASMON-DRIVEN REACTIONS OF 4-MERCAPTOPHENYLBORONIC ACID ON SILVER NANOPARTICLES: A SERS STUDY

DOI: 10.66951/OVPY1367; https://doi.org/10.66951/OVPY1367

Jan Kozisek, kozisekja@natur.cuni.cz
Charles University, Faculty of Science, Department of Physical and Macromolecular Chemistry, Hlavova 2030, 128 40 Prague 2, Czech Republic

Ivana Sloufova, sloufovi@natur.cuni.cz
Charles University, Faculty of Science, Department of Physical and Macromolecular Chemistry, Hlavova 2030, 128 40 Prague 2, Czech Republic

Abstract

This work presents a preliminary SERS spectroscopy screening of plasmon-induced transformations of arylboronic compounds on silver-based nanostructures. The primary objective was to evaluate the feasibility of monitoring the Suzuki–Miyaura cross-coupling reaction (SMCR) on an exploratory AgPd bimetallic substrate under 532 nm excitation, aiming to overcome the high intrinsic plasmon damping of conventional transition-metal catalysts. Initial trends indicate that transitioning from strongly chemisorbed to weakly bound, physisorbed reactants successfully resolve spectral ambiguities and enhance reaction pathways. Additionally, baseline tracking of independent 4-mercaptophenylboronic acid (MPBA) behavior under basic conditions revealed pronounced side reactions; along with expected protodeboronation, unexpected homocoupling to 4,4′-biphenyldithiol and a nitration pathway driven by residual nitrite species were identified. Overall, these initial models demonstrate the potential of silver-assisted plasmonic substrates for the exploratory tracking of transition-metal-catalyzed surface reactions.

1 Introduction

Plasmon-driven reactions have emerged as a significant field of study over the past two decades, largely enabled by plasmon-enhanced spectroscopies on nanostructured materials. When electron oscillations are confined to a nanostructure, localized surface plasmon resonance (LSPR) occurs, which can both enhance chemical reactivity and enable monitoring of surface reactions as well [1]. A typical system for studying plasmonic reactions via surface-enhanced Raman scattering (SERS) spectroscopy relies on anchored substrates via a thiol group to the surface of the plasmonic material. Well-studied benchmark reactions include the conversion of 4-nitrothiophenol (NTP) to 4,4′-dimercaptoazobenzene (DMAB) [2] and the reduction of NO_2 groups to NH_2 in dinitroazobenzene compounds [3]. Cross-coupling reactions, such as the Suzuki-Miyaura cross-coupling reaction (SMCR), which forms biaryl compounds from aryl boronic acids and aryl halides, are also of high interest [4,5].

The primary mechanisms driving plasmonic catalysis are the hot carrier mechanism and the thermal pathway, alongside direct charge transfer as a distinct mechanism. To distinguish between hot carrier and thermal mechanisms, kinetic data fitting is commonly employed: the fitting curve for the hot carrier mechanism follows a linear function, whereas the thermal mechanism is characterized by an exponential function [6].

The primary objective of this study was to optimize the SMCR for real-time SERS monitoring on hydroxylamine-reduced silver nanoparticles (AgNH). Although the SMCR conventionally proceeds in non-aqueous media, its feasibility in eco-friendly aqueous environments catalyzed by AgPd

nanoparticles [7] and on palladium (Pd) or bimetallic gold-palladium (AuPd) nanoparticles together with monitoring the reaction by SERS had already been documented [1]. Nevertheless, neither AgPd, AuPd nor Pd nanoparticles are substrates achieving high SERS enhancement. Therefore, in this study we tried adapting this transition metal catalysis to a silver-based plasmonic substrate for SERS investigation. We investigate the chemical behavior of 4-mercaptophenylboronic acid (MPBA) on silver nanoparticles, focusing on the undesirable deboronation reaction that leads to the loss of the reactive $–B(OH)_2$ group [8,9]. To find ways to suppress this reaction, SERS was utilized to monitor MPBA deboronation under various experimental conditions. Surprisingly, we detected not only the expected product, thiophenol (TP), but also other reaction products such as 4,4′-biphenyldithiol (BPDT) resulting from a plasmon-driven homocoupling pathway, and in some cases, NTP. The latter points to an unexpected nitration reaction driven by residual nitrite species from the nanoparticle synthesis [8].

2 Results and Discussion

2.1 Characterization of SERS active systems and initial SMCR studies

To establish a suitable catalytic platform for monitoring the SMCR via SERS spectroscopy, initial feasibility studies focused on balancing surface conditions and reactant binding. A bimetallic framework consisting of palladium-modified silver nanoparticles (AgNH/Pd) was prepared as an exploratory substrate. Preliminary TEM (**Figure 1.**) and XPS (**Figure 2.**) measurements provided baseline confirmation of the decoration of AgNH with Pd species. Furthermore, UV-Vis spectroscopy revealed a qualitative redshift in the localized surface plasmon resonance (LSPR) maximum from 411 nm for bare AgNH to 423 nm after the addition of Pd ions, indicating a clear modification of the nanoparticle surface. All exploratory SERS evaluations were conducted under 532 nm laser excitation.

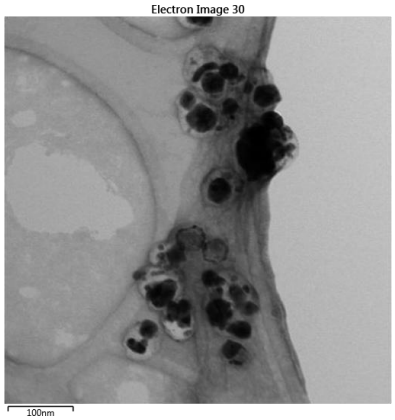


Figure 1. TEM micrograph of AgNH/Pd NPs.

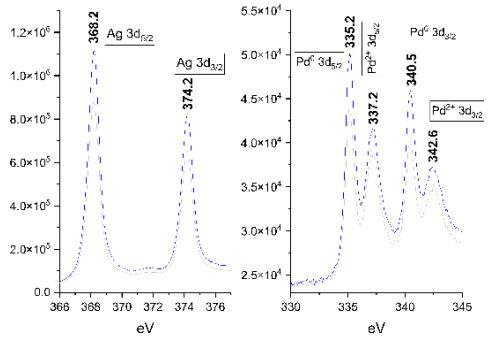


Figure 2. XPS spectra of AgNH/Pd NPs.

In the initial screening phase, the reaction was evaluated using a fully chemisorbed model system consisting of AgNH treated with MPBA, 4-bromothiophenol (BTP), an aqueous NaOH base, and a K_2PdCl_4 ([Pd]) catalyst source (**Figure 3.**). However, under these preliminary testing conditions, the spectral fingerprints of the cross-coupling and competing homocoupling pathways (Scheme 1) could not be unambiguously differentiated; in these initial trials, BPDT emerged as the dominant spectral product. To address this ambiguity in subsequent proof-of-concept tests, MPBA was replaced with phenylboronic acid (PBA), which lacks the thiol anchoring group. This modified system AgNH/BPT/PBA/NaOH/[Pd]) successfully yielded spectral features consistent with the distinct SMCR cross-coupling product, biphenyl-4-thiol (BPT) (**Figure 4.**), offering a preliminary baseline for comparison with literature data where Au/Pd nanoparticles were utilized as catalysts [4].

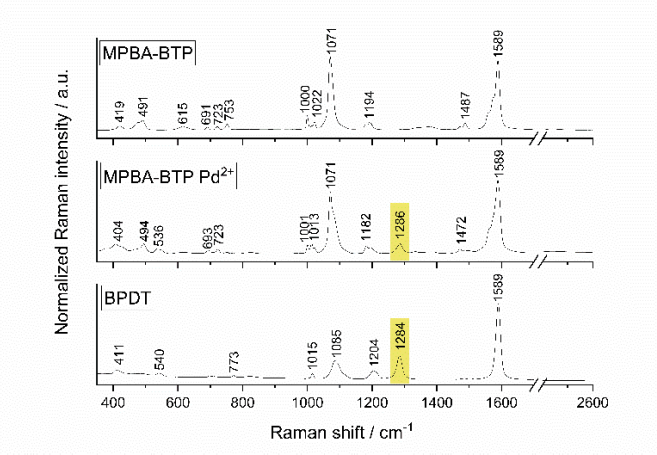


Figure 3. SERS spectra of reaction mixture before after reaction and standard spectrum of biphenyl.

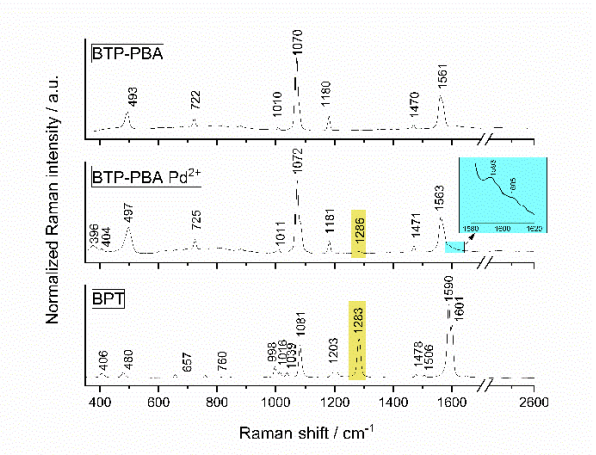
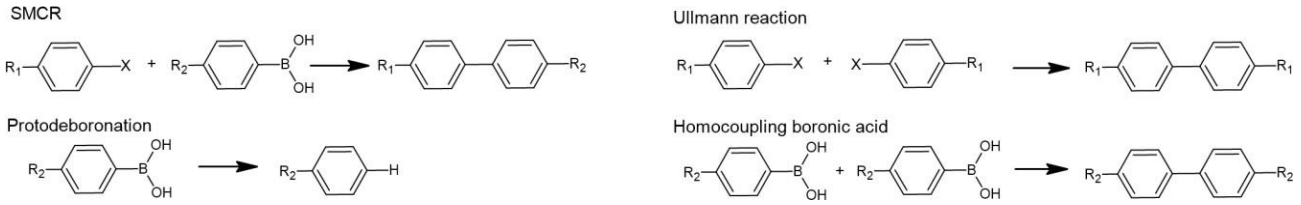


Figure 4. SERS spectra of reaction mixture addition of catalyst, before addition catalyst, after reaction and standard spectrum of biphenyl.



Scheme 1 – Scheme of SMCR and s side reactions.

22 Optimization: Transition from chemisorbed to physisorbed reactants

Based on initial observations suggesting that replacing strongly chemisorbed reactants might influence reaction kinetics, a preliminary screening strategy was altered by shifting from a strongly chemisorbed (thiol-anchored) state to a weaker bound or physisorbed state.

For these exploratory trials, BTP was replaced with 4-iodobenzonitrile (IBN), and MPBA was substituted with either PBA or 4-(methylthio)phenylboronic acid (MTPBA). Two new reaction series were monitored to assess qualitative trends using AgNH, the respective reactants, bases (NaOH or K_2CO_3), and [Pd] catalyst: (i) The PBA series: AgNH + IBN + PBA + bases + [Pd] (**Figure 5., 6.**), which indicated spectral features corresponding to 4-cyanobiphenyl as the potential SMCR product.

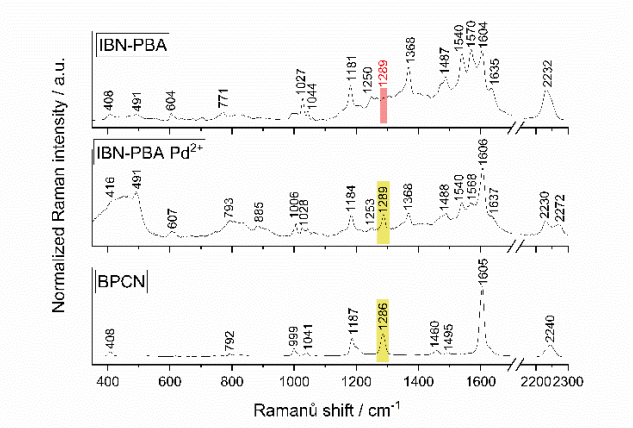


Figure 5. SERS spectra of reaction mixture with before addition of catalyst, after reaction spectrum of biphenyl.

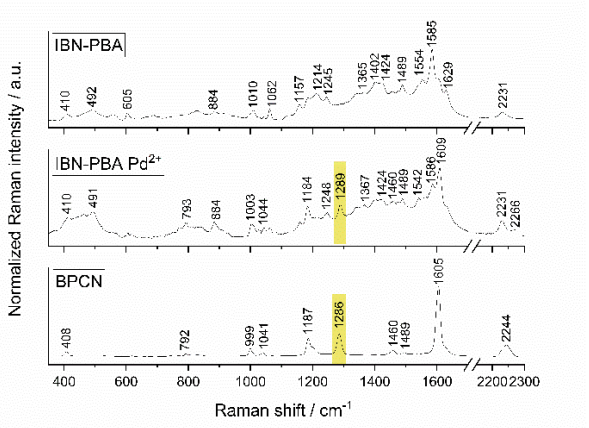


Figure 6. SERS spectra of reaction mixture with NaOH K2CO3 before addition catalyst, after reaction and standard and standard spectrum of biphenyl.

(ii) The MTPBA series: AgNH + IBN + MTBA + bases + [Pd] (**Figure 7., 8.**), which showed trends toward the formation of 4′-(methylthio)biphenyl-4-carbonitrile. In these preliminary screening steps, the series utilizing IBN qualitatively suggested a faster spectral evolution compared to the thiol-anchored precursors. However, when K_2CO_3 was introduced as the base in combination with IBN, spectral indications of a competing Ullmann-type homocoupling pathway were detected in both test systems.

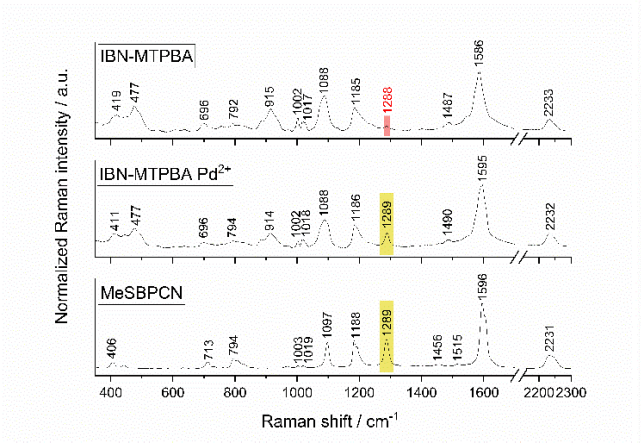


Figure 7. SERS spectra of reaction mixture with before addition of catalyst, after reaction spectrum of biphenyl.

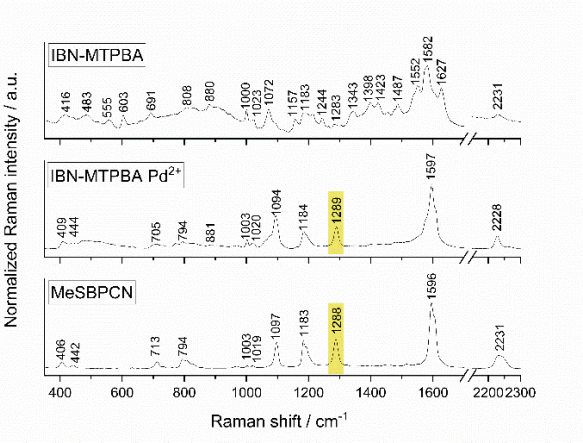


Figure 8. SERS spectra of reaction mixture with NaOH K2CO3 before addition catalyst, after reaction and standard and standard spectrum of biphenyl.

Ultimately, these initial screening models indicated that the 532 nm excitation wavelength is a promising candidate for this platform, providing sufficient SERS enhancement for baseline evaluation with viable signal-to-noise ratios and short accumulation times. This performance highlights the potential of silver-based substrates over conventional catalytic platforms based on pure Pd or Au/Pd nanoparticles. While silver possesses exceptional plasmonic efficiency in the visible range, transition metals like Pd and their alloys with gold suffer from high intrinsic damping and unfavorable dielectric properties in this spectral region [10,11].

2.3 MPBA side reactions

In parallel, the independent chemical behavior of MPBA on bare AgNH under basic conditions was studied to clarify the background processes. Importantly, it was found that chemisorbed MPBA on AgNH under 532 nm excitation exhibits pronounced side reactions, most notably deboronation. While this laser-induced protodeboronation of MPBA is well-documented in the literature [9], our SERS experiments revealed additional, unexpected spectral features.

Apart from the expected deboronation, we observed bands around 1280 cm^{-1} corresponding to the C–C inter-ring vibration of BPDT, confirming a plasmon-driven homocoupling pathway (not shown here, [8]). More surprisingly, an intense band at approximately 1330 cm^{-1} appeared in several spectra, which was assigned to the symmetric stretching mode of a nitro group NO_2. Subsequent factor analysis isolated a spectral component matching the reference spectrum of 4-nitrothiophenol (NTP) [8]. To determine the origin of this unexpected nitration, we first tested nitrate ions (NO_3^-), as $AgNO_3$ is used during the synthesis of AgNH; however, the addition of KNO_3 did not induce the appearance of the nitro band. The only other nitrogen-containing compound in the system was the reducing agent, hydroxylamine hydrochloride. According to the literature [12,13], the autooxidation of hydroxylamine yields nitrite anions (NO_2^-). To confirm our hypothesis that the reducing agent acts as the ultimate source of the nitro group, we used freshly prepared AgNH, and the 1330 cm^{-1} band was clearly detected in the AgNH/MPBA system. Finally, this mechanism was verified by the intentional addition of sodium nitrite ($NaNO_2$), which successfully replicated the nitration reaction [9].

3 Summary and further research

In this work, a bimetallic AgNH /Pd platform was pre-screened for monitoring the Suzuki- Miyaura cross-coupling reaction (SMCR) via SERS spectroscopy under 532 nm excitation. Preliminary trials showed that shifting from strongly chemisorbed to weakly bound reactants (using IBN) successfully resolves spectral ambiguities and improves reaction trends. This approach takes advantage of silver's higher plasmonic efficiency upon excitation in the visible region compared to Pd or Au/Pd systems. Furthermore, preliminary studies of the behavior of isolated MPBAs revealed significant side reactions, including protodeboration and an unexpected nitration pathway triggered by residual nitrites.

Future research will focus on the comprehensive, quantitative optimization of this bimetallic platform. Detailed kinetic studies are underway to precisely evaluate the impact of reaction conditions (laser power, temperature, and base strength) on reaction yields, alongside advanced chemometric modeling to resolve overlapping spectral features for a definitive publication.

4 Acknowledgement

This work has been funded by a grant from the Programme Johannes Amos Comenius under the Ministry of Education, Youth and Sports of the Czech Republic CZ.02.01.01/00/22_008/0004558 Advanced MUltiscaLe materials for key EnablingTechnologies.

5 References

[1] J. Zhao, J. Wang, A. J. Brock, H. Zhu, J. Photochem. Photobiol. C Photochem. Rev. 2022, 52, 100539

[2] B. Dong, Y. Fang, X. Chen, H. Xu, M. Sun Langmuir 2011, 27, 10677-10682.

[3] L. Cui, P. Wang, Y. Fang, Y. Li, M. Sun, Sci. Rep. 2015, 5, 11920.

[4] Y. Zhao, L. Du, H. Li, W. Xie, J. Chen, J. Phys. Chem. Lett. 2019, 10 (6), 1286–1291

[5] D. S. Lopes, E. V. Miranda, R.A. Ando, P. Corio, Environ. Sci. Nano 2023, 10 (7), 1920−1931

[6] G. Baffou, I. Bordacchini, A. Baldi, R. Quidant, Light Sci. Appl. 2020, 9, 1–16

[7] R. Bayan, N. Karak, ACS Omega 2017, 2, 8868−8876

[8] J. Kozisek, J. Hrncirova, M. Slouf, I. Sloufova, Spectrochim. Acta A Mol. Biomol. Spectrosc. 2024, 319, 124523.

[9] L.T.M. Huynh, H.D. Trinh, S. Lee, S. Yoon, Nanoscale 2020, 12, 24062–24069

[10] S. De Marchi, S. Núñez-Sánchez, G. Bodelón, J. Pérez-Juste, I. Pastoriza-Santos, Nanoscale 2020, 12, 23424–23443

[11] K. Zhang, Y. Xiang, X. Wu, L. Feng, W. He, J. Liu, W. Zhou, S. Xie, Langmuir 2009, 25, 1162- 1168

[12] K.G.G.C. De Silva, M.I. Ranasinghe, S. Chowdhury, React. Kinet. Mech. Catal. 2020, 131, 965–977

[13] M.N. Hughes, H.G. Nicklin, J. Chem. Soc. A Inorganic, Phys, Theor. Chem. 1971, 164–168

DEVELOPMENT OF HYBRID ANTIMICROBIAL PLATFORMS VIA COORDINATION CHEMISTRY

DOI: 10.66951/BRWX2380; https://doi.org/10.66951/BRWX2380

Viktorie Neubertová, viki.kivi21@gmail.com
Centre for Nanomaterials and Biotechnology, Faculty of Science, University of Jan Evangelista Purkyně, Pasteurova 15, 400 96, Ústí nad Labem, Czech Republic

Silvie Rimpelová, silvie.rimpelova@vscht.cz
Department of Biochemistry and Microbiology, Faculty of Food and Biochemical Technology, University of Chemistry and Technology Prague, Technická 1903/3, 166 28 Prague, Czech Republic

Zdeňka Kolská, zdenka.kolska@ujep.cz
Centre for Nanomaterials and Biotechnology, Faculty of Science, University of Jan Evangelista Purkyně, Pasteurova 15, 400 96, Ústí nad Labem, Czech Republic

Abstract

Antimicrobial resistance is driving the search for materials that deliver bactericidal agents with spatial and temporal control. Coordination chemistry offers a versatile approach, because bonds between metal centers and nitrogen-donor linkers combine structural tunability with stimuli-dependent stability. Two hybrid antimicrobial platforms are presented: zeolitic imidazolate framework-8 (ZIF-8) loaded in situ with essential oil components eucalyptol or thymol, and a silver coordination polymer (Ag-CP) grown on chitosan-coated surgical steel. In ZIF-8, the host-to-guest stoichiometry determined morphology, colloidal behavior and release, while in the Ag-CP coating the metal-to-ligand ratio determined surface architecture and silver ion release. Eucalyptol-loaded ZIF-8 inhibited *Staphylococcus epidermidis* and *Escherichia coli* more effectively than thymol-loaded samples, which suffered from pore blocking and aggregation. The equimolar Ag-CP coating remained cytocompatibility at physiological pH and turned bactericidal under mildly acidic conditions. These results support coordination chemistry as a unifying strategy linking porous carriers with functional antimicrobial surfaces.

1 Introduction

Bacterial infections that no longer respond to antibiotics represent one of the pressing challenges in modern medicine, and mortality projections related to antibiotic resistance in the coming decades further highlight the urgency of implementing alternative antibacterial strategies [1,2]. Traditional antibiotic therapy is increasingly being supplemented by approaches based on materials in which the antibacterial effect is incorporated into a solid carrier or surface, rather than being administered as a free active ingredient [3,4]. Such approaches allow the active species to be localized, protected, and ideally released only when and where it is required.

Coordination chemistry provides a particularly flexible basis for this purpose. Materials composed of metal ions and organic linking units, including metal-organic frameworks (MOFs) and coordination polymers, combine high structural order with porosity and surface chemistry that can be tuned during synthesis [5–7]. Two features make them interesting for antibacterial use. First, several of the metal centers commonly used, among them Zn^{2+}, Ag^{+} and Cu^{2+}, are themselves bactericidal, so the framework can act at once as a structural host and a source of active ions [7,8]. Second, the bonds between metal centers and nitrogen-donor linkers such as 2-methylimidazole are sensitive to

protonation, so the assembly remains stable at physiological pH but dissociates in acidic environments [9,10]. Because bacterial colonization and biofilm formation lower the local pH through the secretion of organic acids, this acid sensitivity can be exploited as a trigger that induces release to the presence of infection [11–13].

In this context, two material archetypes are particularly important. Porous frameworks such as ZIF-8 offer a large pore volume in which guest molecules can be stored and from which they are released upon framework breakdown, which makes them suitable nanocarriers for antibacterial agents [5,9,14]. Among the potential substances, the components of essential oils have gained attention because they come from natural sources and affect bacterial membranes, although their volatility and low water solubility complicate their direct use [15,16]. Encapsulation in a porous matrix can mitigate these disadvantages by restricting the movement of the volatile molecule and slowing its release [14,17]. The second archetype relates to coordination polymers grown on a metal surface, which is important for preventing implant-associated infections. Stainless steel is widely used for load-bearing implants, but it is not resistant to localized corrosion or bacterial colonization *in vivo* [18,19]. Silver is a proven broad-spectrum antibacterial agent with a low tendency to induce resistance, but coatings based on physically adsorbed silver often release it in uncontrolled doses that are short-lived and locally toxic [20,21]. Trapping silver in such a coordination polymer, anchored via a chitosan interlayer that both promotes adhesion and chelates metal ions, offers a path to more controlled behavior [22–24].

The aim of this paper is to provide a comprehensive overview of the development of these two hybrid antimicrobial platforms and to identify the design principles they have in common. Here, we summarize the synthetic rationale, relevant literature, and results that demonstrate how coordination chemistry can be used to achieve controlled antibacterial activity.

2 Platform development and antibacterial evaluation

2.1 Porous frameworks as carriers for essential oil components

ZIF-8, built from Zn^{2+} nodes linked with 2-methylimidazolate, offers well-defined microporosity and high chemical stability, making it a suitable nanocarrier for volatile antibacterial molecules [5]. Two essential oil components with contrasting properties were selected as guests: (i) eucalyptol, a cyclic ether with moderate antibacterial activity, and (ii) thymol, a phenolic monoterpenoid with stronger intrinsic potency [15,16]. The resulting composites are denoted ZIF-8-EUC and ZIF-8-THY according to the encapsulated guest.

Powder X-ray diffraction confirmed retention of the sodalite ZIF-8 topology in both composites, with no evidence of guest coordination to zinc by Fourier-transform infrared spectroscopy. Nitrogen sorption and colloidal characterization revealed that ZIF-8-THY blocked the pore network more extensively and showed poorer colloidal stability than ZIF-8-EUC, consistent with the aggregation behavior observed in suspension.

The most important differences appeared in antibacterial performance (**Figure 1.**), assessed against *Escherichia coli* (*E. coli*) and *Staphylococcus epidermidis* (*S. epidermidis*) by the drop method. Pristine ZIF-8 was only weakly active against the Gram-positive strain but inhibited *E. coli* more effectively. Loading with eucalyptol (ZIF-8-EUC) improved performance against both strains in a concentration-dependent manner. This contrast follows from colloidal and textural behavior, because the pore blocking and aggregation caused by thymol restrict its release and keep the extracellular concentration below the level needed to disrupt bacterial membranes [25].

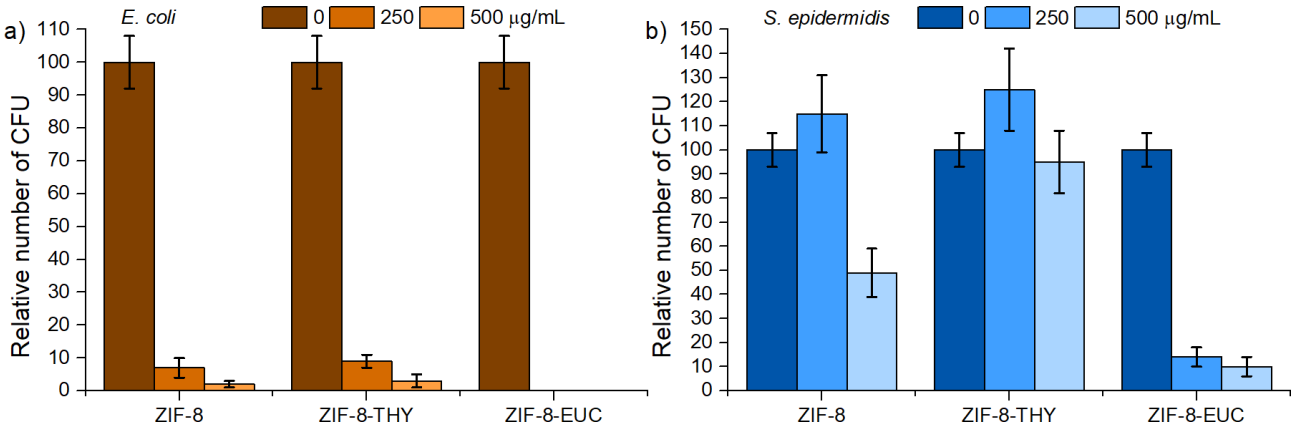


Figure 1. Relative number of CFU for pristine ZIF-8, ZIF-8-THY and ZIF-8-EUC against (a) E. coli and (b) S. epidermidis at different concentrations of samples.

2.2 Silver coordination polymer coatings on chitosan-coated surgical steel

The second platform applies the same principles of coordination chemistry to a functional surface. Surgical steel substrates were first coated with chitosan, a cationic polysaccharide whose amine and hydroxyl groups improve adhesion and sequester metal ions [22,23]. A silver coordination polymer (Ag-CP), formed from silver nitrate and 2-methylimidazole, was then grown *in situ* on this interlayer. The silver-to-ligand ratio was tuned to control the architecture of the deposited phase, and an equimolar formulation producing discrete clusters on the chitosan interlayer was identified as the most favorable [10,24]. Infrared spectroscopy confirmed Ag-CP formation through the band assigned to the Ag-N coordination bond.

The antibacterial and cytotoxic responses depended strongly on this architecture, and the equimolar Ag-CP coating proved the most useful (**Figure 2.**). At physiological pH it was only moderately inhibitory, yet under the mildly acidic conditions associated with infection the same coating eradicated both strains completely (**Figure 2a**). This on-demand switch arises from two cooperative events. Protonation and swelling of the chitosan interlayer, combined with acid-induced dissociation of the silver-imidazole coordination bonds, together release silver ions only where they are needed [9,11]. The equimolar Ag-CP coating also remained cytocompatibility toward fibroblasts at physiological pH (**Figure 2b**). As with the porous carriers, structural stability rather than sheer silver content determined whether the material behaved in a controlled manner [21,26].

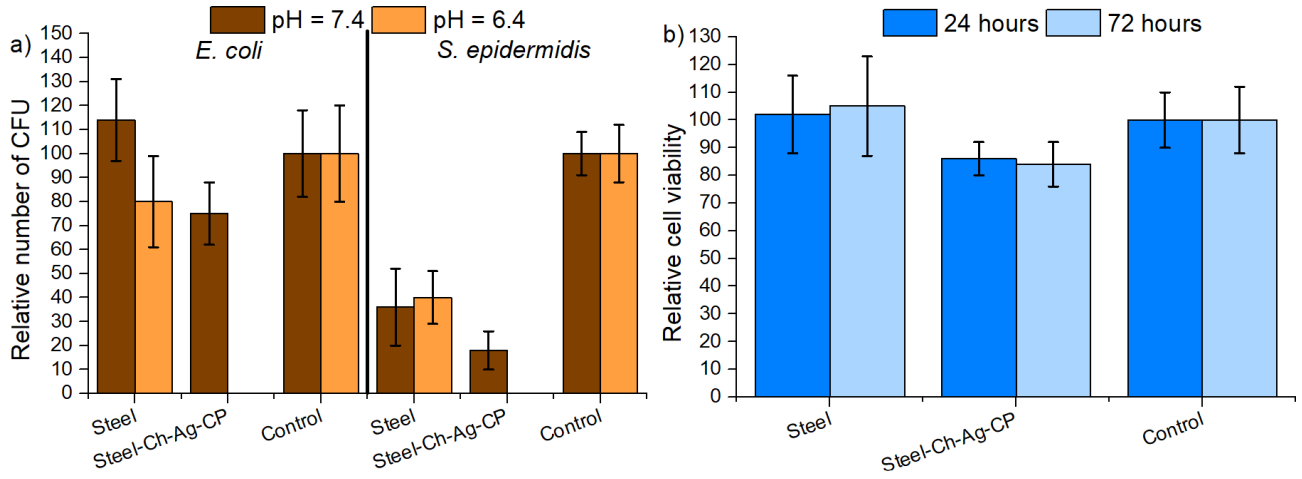


Figure 2. (a) Antibacterial activity against *E. coli* and *S. epidermidis* at physiological pH = 7.4 and at pH = 6.4, (b) cell viability after 24 and 72 hours.

3 Conclusions

Two hybrid antimicrobial platforms were developed on a shared coordination-chemistry foundation: (i) ZIF-8 nanocarriers loaded with essential oil components, and (ii) a silver coordination polymer grown on chitosan-coated surgical steel. In ZIF-8, the host-to-guest stoichiometry controlled the structure, colloidal stability and release of the encapsulated compounds, while in the Ag-CP coating the metal-to-ligand ratio determined the surface architecture and the pattern of silver ion release. Eucalyptol proved more effective than thymol as a ZIF-8 guest because it was released more readily, and the equimolar Ag-CP coating combined cytocompatibility at physiological pH with potent, infection-triggered bactericidal activity. Taken together, these results indicate that controlled antibacterial behavior depends less on the intrinsic potency of the active agent than on the stability and release characteristics imparted by the coordination environment. Future work will focus on extended concentration ranges, additional sample variants, and systematic release quantification to further optimize both platforms.

4 Acknowledgement

This work has been funded by a grant from the Programme Johannes Amos Comenius under the Ministry of Education, Youth and Sports of the Czech Republic CZ.02.01.01/00/22_008/0004558 Advanced MUltiscaLe materials for key Enabling Technologies.

5 References

[1] Kariuki S. Global burden of antimicrobial resistance and forecasts to 2050. The Lancet 2024;404:1172–3. https://doi.org/10.1016/S0140-6736(24)01885-3.

[2] Okeke IN, De Kraker MEA, Van Boeckel TP, et al. The scope of the antimicrobial resistance challenge. The Lancet 2024;403:2426–38. https://doi.org/10.1016/S0140-6736(24)00876-6.

[3] Arshadi Edlo A, Akhbari K, Henry DJ. Beyond antibiotics: novel solutions to address antibacterial resistance. Mater Adv 2025;6:7662–84. https://doi.org/10.1039/D5MA00552C.

[4] Wang C, Wei X, Zhong L, et al. Metal-Based Approaches for the Fight against Antimicrobial Resistance: Mechanisms, Opportunities, and Challenges. J Am Chem Soc 2025;147:12361–80. https://doi.org/10.1021/jacs.4c16035.

[5] Park KS, Ni Z, Côté AP, et al. Exceptional chemical and thermal stability of zeolitic imidazolate frameworks. Proc Natl Acad Sci USA 2006;103:10186–91. https://doi.org/10.1073/pnas.0602439103.

[6] Wu M, Yang Y. Metal–Organic Framework (MOF)-Based Drug/Cargo Delivery and Cancer Therapy. Advanced Materials 2017;29:1606134. https://doi.org/10.1002/adma.201606134.

[7] Tian Y, Wang B, Zhang Z, et al. Recent advances in metal–organic frameworks for antibacterial applications: mechanisms and emerging strategies. RSC Adv 2025;15:26710–27. https://doi.org/10.1039/D5RA02955D.

[8] Yan D, Yang M, Cheng F, et al. Novel antimicrobial agents prepared on the basis of metal- organic frameworks (MOFs) and their applications in the food field. Trends in Food Science & Technology 2025;161:105070. https://doi.org/10.1016/j.tifs.2025.105070.

[9] Sun C-Y, Qin C, Wang X-L, et al. Zeolitic imidazolate framework-8 as efficient pH-sensitive drug delivery vehicle. Dalton Trans 2012;41:6906. https://doi.org/10.1039/c2dt30357d.

[10] Seyedpour SF, Arabi Shamsabadi A, Khoshhal Salestan S, et al. Tailoring the Biocidal Activity of Novel Silver-Based Metal Azolate Frameworks. ACS Sustainable Chem Eng 2020;8:7588–99. https://doi.org/10.1021/acssuschemeng.0c00201.

[11] Radovic-Moreno AF, Lu TK, Puscasu VA, et al. Surface Charge-Switching Polymeric Nanoparticles for Bacterial Cell Wall-Targeted Delivery of Antibiotics. ACS Nano 2012;6:4279–87. https://doi.org/10.1021/nn3008383.

[12] Zhang T, Liu Q, Meng F, et al. Recent advances in stimuli-responsive antibacterial coatings: Bacteria-killing and releasing mechanism, design strategies, and potential applications. Progress in Organic Coatings 2024;186:107923. https://doi.org/10.1016/j.porgcoat.2023.107923.

[13] Wang X, Shan M, Zhang S, et al. Stimuli-Responsive Antibacterial Materials: Molecular Structures, Design Principles, and Biomedical Applications. Advanced Science 2022;9:2104843. https://doi.org/10.1002/advs.202104843.

[14] Angeli GK, Kotzabasaki MI, Maraveas C. Metal Organic Frameworks for Smart Storage and Delivery of Aromatic Volatiles and Essential Oils in Agrifood. Applied Sciences 2025;15:5479. https://doi.org/10.3390/app15105479.

[15] Yao B, He B, Peng J, et al. The comprehensive review of eucalyptol: synthesis, metabolism, and therapeutic applications in disease treatment. Mol Biol Rep 2025;52:346. https://doi.org/10.1007/s11033-025-10461-y.

[16] Modareskia M, Fattahi M, Mirjalili MH. Thymol screening, phenolic contents, antioxidant and antibacterial activities of Iranian populations of Trachyspermum ammi (L.) Sprague (Apiaceae). Sci Rep 2022;12:15645. https://doi.org/10.1038/s41598-022-19594-7.

[17] Hernández-López R, Cuellar-Sánchez JÁ, López-Malo A, et al. Synthesis, characterization and evaluation of ZIF-8/CMC composites loaded with eugenol for sustained antimicrobial activity. Cellulose 2025;32:8371–93. https://doi.org/10.1007/s10570-025-06718-1.

[18] Sultana N, Nishina Y, Nizami MZI. Surface Modifications of Medical Grade Stainless Steel. Coatings 2024;14:248. https://doi.org/10.3390/coatings14030248.

[19] Chew K-K, Zein SHS, Ahmad AL. The corrosion scenario in human body: Stainless steel 316L orthopaedic implants. NS 2012;04:184–8. https://doi.org/10.4236/ns.2012.43027.

[20] Stensberg MC, Wei Q, McLamore ES, et al. Toxicological Studies on Silver Nanoparticles: Challenges and Opportunities in Assessment, Monitoring and Imaging. Nanomedicine 2011;6:879–98. https://doi.org/10.2217/nnm.11.78.

[21] Feng QL, Wu J, Chen GQ, et al. A mechanistic study of the antibacterial effect of silver ions onEscherichia coli andStaphylococcus aureus. J Biomed Mater Res 2000;52:662–8. https://doi.org/10.1002/1097-4636(20001215)52:4%3C662::AID-JBM10%3E3.0.CO;2-3.

[22] Marsico M, Azari R, Curcio M, et al. Enhancing the Antibacterial Properties of Chitosan Coatings: Ag@Chitosan and Chitosan from Insects. Coatings 2024;14:925. https://doi.org/10.3390/coatings14080925.

[23] Qin Y, Zhu C, Chen J, et al. The absorption and release of silver and zinc ions by chitosan fibers. J of Applied Polymer Sci 2006;101:766–71. https://doi.org/10.1002/app.23985.

[24] Gordon O, Vig Slenters T, Brunetto PS, et al. Silver Coordination Polymers for Prevention of Implant Infection: Thiol Interaction, Impact on Respiratory Chain Enzymes, and Hydroxyl Radical Induction. Antimicrob Agents Chemother 2010;54:4208–18. https://doi.org/10.1128/AAC.01830-09.

[25] Muthalagu S, Natarajan S. Deciphering the Antimicrobial and Antibiofilm Efficiency of Thyme Essential Oil

Encapsulated Zeolitic Imidazole Framework-8 Against Foodborne Pathogens. Curr Microbiol 2025;82:49. https://doi.org/10.1007/s00284-024-04025-9.

[26] Slavin YN, Asnis J, Häfeli UO, et al. Metal nanoparticles: understanding the mechanisms behind antibacterial activity. J Nanobiotechnol 2017;15:65. https://doi.org/10.1186/s12951-017- 0308-z.

TRANSITION METAL DICHALCOGENIDE NANOSCROLLS: STRUCTURE, PROPERTIES AND EMERGING APPLICATIONS

DOI: 10.66951/WAHB7133; https://doi.org/10.66951/WAHB7133

Rahul Kesarwani, rahul.kesarwani@matfyz.cuni.cz
Department of Condensed Matter Physics, Faculty of Mathematics and Physics, Ke Karlovu 5, 121 16 Prague, Czechia
Department of Low-dimensional Systems, Heyrovsky Institute, Dolejskova 3, 182 00 Prague, Czechia

Jana Vejpravová, jana.vejpravova@matfyz.cuni.cz
Department of Condensed Matter Physics, Faculty of Mathematics and Physics, Ke Karlovu 5, 121 16 Prague, Czechia

Abstract

Transition metal dichalcogenide (TMD) nanoscrolls represent a unique class of curved two-dimensional (2D) materials, combining an open topology with tunable interlayer coupling, curvature, and local strain. This mini-review summarizes recent advances in their fabrication, structural and optical properties, and emerging photonic applications. Particular attention is given to enhanced light–matter interactions, polarization-dependent optical response, and recent developments in chiral and Janus nanoscrolls, highlighting their potential for future optoelectronic and quantum technologies.

1 Introduction

Transition metal dichalcogenides (TMDs) have emerged as one of the most extensively studied families of 2D materials owing to their diverse electronic, optical, mechanical, and catalytic properties. Depending on their composition and crystal structure, TMDs exhibit semiconducting, metallic, superconducting, or magnetic behavior, making them highly versatile platforms for both fundamental research and technological applications. Their reduced dimensionality further enables strong light–matter interactions, pronounced excitonic effects, and exceptional mechanical flexibility, offering unique opportunities for tailoring material properties beyond those accessible in conventional bulk crystals [1,2].

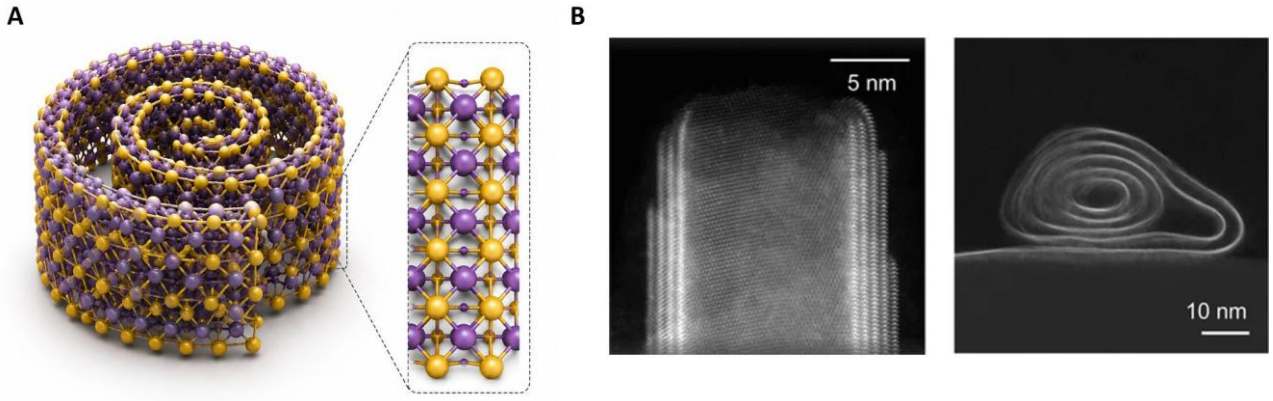


Figure 1. (A) Schematic illustration of a TMD nanoscroll; the yellow and violet spheres represent the chalcogen and transition-metal atoms, respectively. (B) HR-TEM image of a Janus TMD nanoscroll obtained by a liquid- induced rolling method. Adapted from [10].

While most studies have focused on atomically flat TMD layers, increasing attention has recently been devoted to intentionally introducing three-dimensional architecture. Controlled deformation of 2D crystals through folding, wrinkling, bending, or scrolling provides an effective route for engineering local strain, modifying interlayer interactions, and tailoring electronic and optical properties without altering the chemical composition of the material. Such geometrical design has therefore emerged as an important strategy for expanding the functionality of layered materials [3].

Among the various curved architectures, nanoscrolls occupy a particularly unique position. Unlike closed nanotubes, nanoscrolls possess an open spiral topology formed by rolling a two-dimensional sheet into a spiral without forming covalent bonds between the overlapping layers. This open geometry combines the advantages of planar monolayers and tubular nanostructures while introducing additional degrees of freedom, including tunable inner diameter, variable interlayer spacing, and accessible internal surfaces. As a consequence, nanoscrolls exhibit highly inhomogeneous strain distributions, modified dielectric environments, and altered electromagnetic field confinement, all of which can substantially influence their physical properties [4–6].

These distinctive structural characteristics have stimulated growing interest in TMD nanoscrolls over the past decade. Considerable progress has been achieved in developing reliable fabrication strategies, ranging from strain-driven self-scrolling and solvent-assisted approaches to increasingly controlled synthesis routes. At the same time, both theoretical and experimental studies have revealed that scrolling can significantly modify electronic band structures, excitonic behavior, vibrational properties, and light–matter interactions. More recently, nanoscrolls have also emerged as promising platforms for enhanced photodetection, polarization-sensitive optoelectronics, and chiral photonic functionalities, highlighting their potential for future quantum and photonic technologies [5–9].

In this mini-review, we summarize recent advances in TMD nanoscrolls, with particular emphasis on the relationship between their unique geometry and resulting physical properties. We first discuss the principal fabrication strategies that enable the formation of TMD nanoscrolls, followed by an overview of the structural, optical, and electromagnetic phenomena arising from their curved morphology. Finally, we highlight representative applications and outline future opportunities for exploiting nanoscrolls in next-generation optoelectronic and quantum material platforms.

2 Fabrication Strategies

Various fabrication strategies for preparing TMD nanoscrolls have been developed, see **Figure 2**. The formation of nanoscrolls is generally governed by the competition between elastic strain energy stored within the two-dimensional sheet and the energetic gain associated with van der Waals interactions between overlapping layers. Once the energy released by scrolling exceeds the bending energy required to deform the crystal, spontaneous rolling becomes energetically favorable. Consequently, many fabrication strategies aim to locally release built-in strain or reduce the energy barrier for scrolling rather than directly forcing the material into a rolled geometry.

One of the most straightforward and widely adopted approaches relies on solvent-assisted scrolling, in which a volatile solvent, such as ethanol, is introduced at the edge of an exfoliated or transferred TMD flake. The infiltration of the solvent weakens the adhesion between the crystal and the substrate while capillary forces initiate rolling from the exposed edge. Following solvent evaporation, stable nanoscrolls are formed with high structural integrity and relatively good reproducibility. Owing to its simplicity and compatibility with conventional sample preparation techniques, this approach has become one of the most employed methods for producing TMD nanoscrolls [5].

Alternative fabrication strategies exploit the release of intrinsic or externally induced strain within atomically thin crystals. Mechanical deformation, transfer-induced stress, thermal treatment, or plasma

processing can generate local strain gradients that promote scrolling once the crystal is partially detached from the supporting substrate. These methods provide additional opportunities to tailor the dimensions and morphology of the resulting nanoscrolls, although precise control over parameters such as diameter, number of windings, or chirality remains challenging. More recently, controlled

fabrication protocols have enabled improved reproducibility and greater flexibility in engineering nanoscroll architecture, opening the possibility of integrating these structures into functional devices [3,5].

More recently, the concept of TMD nanoscrolls has been extended to Janus systems. These advances demonstrate that scrolling is not limited to conventional TMDs but represents a versatile strategy for engineering increasingly complex two-dimensional material architectures [10].

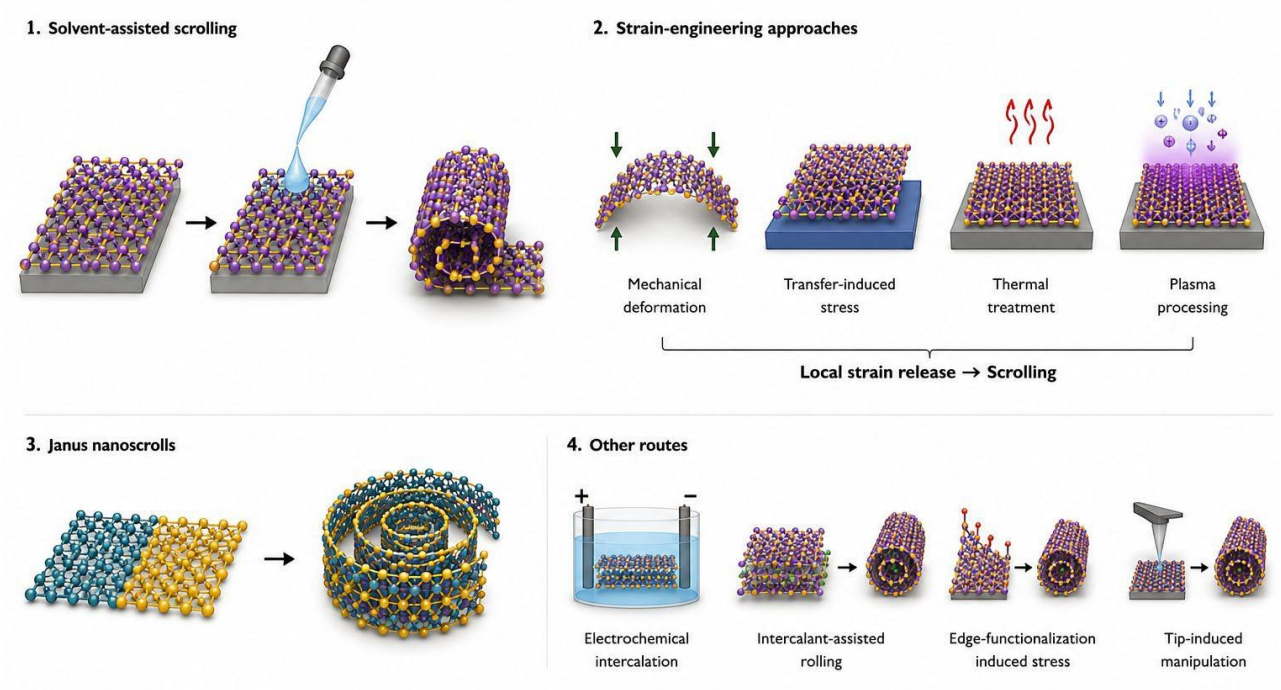


Figure 2. Various fabrication strategies for TMD nanoscrolls.

3 Structure–Property Relationships

3.1 Structural Characteristics

The unique properties of TMD nanoscrolls originate from their open spiral geometry, which distinguishes them from both planar two-dimensional crystals and closed nanotubes. Unlike nanotubes, nanoscrolls do not form covalent bonds between neighboring windings, resulting in an open topology with accessible inner surfaces and enhanced structural flexibility. This geometry enables interactions with the surrounding environment while allowing structural relaxation through variations in the scroll diameter and winding configuration [4,5].

A key structural characteristic of nanoscrolls is the continuous tunable interlayer spacing. Since adjacent windings are held together solely by van der Waals interactions, the interlayer distance depends on the scrolling conditions, local morphology, and external perturbations. This provides an effective route for tailoring interlayer coupling, dielectric screening, and charge transfer without modifying the chemical composition of the material [5].

The rolling process also introduces pronounced curvature and non-uniform strain. In contrast to nanotubes with constant curvature, nanoscrolls exhibit continuously varying local curvature accompanied by tensile and compressive strain across the scroll cross-section. These structural features modify the local electronic structure, vibrational properties, and excitonic behavior, forming the basis for many of the unusual optical phenomena discussed in the following sections [4,6].

Recent developments have further extended the concept of nanoscrolls to Janus transition metal dichalcogenides, where the intrinsic out-of-plane asymmetry of the monolayers is combined with the curvature of the scrolled geometry. Such structures provide additional opportunities for engineering built-in electric fields, piezoelectric response, and electronic properties, opening new directions for designing multifunctional nanoscroll-based architectures [10].

The structural evolution during scrolling has been primarily monitored by Raman spectroscopy. Changes in phonon frequencies, linewidths, and relative mode intensities provide direct insight into local strain, curvature, and interlayer coupling, establishing Raman spectroscopy as a key tool for correlating nanoscroll morphology with their optical and electronic properties [6].

3.2 Optical and Electronic Properties

The structural characteristics of TMD nanoscrolls directly influence their electronic and optical properties through the combined effects of curvature, strain, and modified interlayer interactions. The continuously varying local environment lifts the structural uniformity of planar crystals, leading to spatial modulation of the electronic band structure and dielectric screening. Consequently, nanoscrolls provide an effective platform for engineering light–matter interactions without altering the chemical composition of the material [5,6].

Excitonic transitions are particularly sensitive to the local structural environment. Variations in strain and dielectric screening modify exciton binding energies and recombination dynamics, while the coexistence of regions with different curvature and interlayer coupling gives rise to spatially varying optical responses. These effects are readily observed by photoluminescence spectroscopy through spectral shifts and modified emission intensity compared with planar monolayers [6].

The reduced symmetry of the scrolled geometry also affects the polarization properties of light emission and scattering. Combined with curvature-induced symmetry breaking, anisotropic morphology can produce strongly polarization-dependent optical responses that are absent in flat crystals. Recently, controlled TMD nanorolligami demonstrated exceptionally high linear polarization ratios originating from the chiral geometry of the nanoscrolls, highlighting their potential as compact polarization-selective photonic elements [11].

Beyond modifying the intrinsic optical response, the spiral geometry promotes local electromagnetic field confinement through multiple internal reflections and field localization within the rolled structure. The resulting enhancement of light–matter interaction increases optical absorption, excitation efficiency, and nonlinear optical response, providing an additional route for tailoring the functionality of TMD nanoscrolls [6,7]. These advantages have already been exploited in nanoscroll-based photodetectors, where enhanced optical absorption and efficient carrier separation lead to significantly improved photo response compared with planar devices [8,9].

4 Applications and Outlook

The unique structural characteristics of TMD nanoscrolls have already enabled a range of promising optoelectronic and photonic applications. Enhanced light absorption, efficient carrier separation, and electromagnetic field localization have been successfully exploited to improve the performance of

nanoscroll-based photodetectors, while recent advances in nanorolligami and Janus nanoscrolls have further expanded the available design strategies for multifunctional devices.

Future developments will primarily depend on deterministic fabrication with precise control over the geometry, position, and chirality of individual nanoscrolls. Such advances will facilitate the realization of complex heterostructures and enable systematic engineering of optical and electronic properties through structural design. Particularly attractive directions include the fabrication of nanoscrolls from homo- and heterobilayers, enabling the combination of scrolling with interlayer coupling engineering, as well as the encapsulation of functional materials within the open nanoscroll cavity to create hybrid nano systems with tailored optical, magnetic, or catalytic functionalities.

Another promising opportunity lies in combining nanoscroll architectures with isotope engineering [12]. Isotopically engineered TMDs provide spectroscopic contrast between individual layers while preserving their electronic properties, offering a unique platform for resolving layer-specific strain, phonon behavior, and interlayer interactions in complex scrolled structures. Such approaches could provide unprecedented insight into the relationship between local morphology and physical properties while enabling the rational design of advanced nanoscroll-based devices.

With their open topology, tunable interlayer interactions, and compatibility with a broad range of two-dimensional materials, TMD nanoscrolls represent a versatile platform for next-generation photonic and quantum technologies. Continued advances in synthesis and structural engineering are expected to expand their role in chiral light emitters and detectors, integrated photonic components, and hybrid quantum material systems.

5 Acknowledgement

This work has been funded by a grant from the Programme Johannes Amos Comenius under the Ministry of Education, Youth and Sports of the Czech Republic CZ.02.01.01/00/22_008/0004558 Advanced MUltiscaLe materials for key Enabling Technologies.

6 References

[1] K. F. Mak and J. Shan, Photonics and Optoelectronics of Two-Dimensional Semiconductor Transition Metal Dichalcogenides, Nat. Photonics, **10**, 216–226 (2016).

[2] M. Chhowalla, D. Jena, and H. Zhang, Two-Dimensional Semiconductors for Transistors, Nat. Rev. Mater., **1**, 16052 (2016).

[3] A. Castellanos-Gomez, H. S. J. van der Zant, and G. A. Steele, Folded MoS_2 Layers with Reduced Interlayer Coupling, Nano Res., **7**, 572–578 (2014).

[4] G. Seifert, H. Terrones, M. Terrones, G. Jungnickel, and T. Frauenheim, Structure and Electronic Properties of MoS_2 Nanotubes, Phys. Rev. Lett., **85**, 146–149 (2000).

[5] X. Cui, Z. Kong, E. Gao, D. Huang, Y. Hao, H. Shen, C.-A. Di, Z. Xu, J. Zheng, and D. Zhu, Rolling up Transition Metal Dichalcogenide Nanoscrolls via One Drop of Ethanol, Nat. Commun., **9**, 1301 (2018).

[6] M. Remškar, A. Mrzel, Ž. Skraba, A. Jesih, M. Čeh, J. Demšar, P. Stadelmann, F. Lévy, and D. Mihailovic, Self-Assembly of Subnanometer-Diameter Single-Wall MoS_2 Nanotubes, Science, **292**, 479–481 (2001).

[7] L. Yadgarov and R. Tenne, Nanotubes from Transition Metal Dichalcogenides: Recent Progress in the Synthesis, Characterization and Electrooptical Properties, Small, **21**, 2400503 (2025).

[8] Y. Wang, X. Li, Z. Wang, Y. Zhang, Y. Liu, and Y. Fang, Transition Metal Dichalcogenide Nanoscroll-Based Photodetectors with Enhanced Photoresponse, Nano Res., **13**, 3286–3293 (2020).

[9] Y. Li, H. Zhang, X. Chen, Y. Zhao, Z. Wang, and J. Li, High-Performance MoS_2 Nanoscroll Photodetectors with Enhanced Light Absorption, ACS Appl. Mater. Interfaces, **15**, 1203–1212 (2023).

[10] M. Kaneda, W. Zhang, Z. Liu, Y. Gao, M. Maruyama, Y. Nakanishi, H. Nakajo, Y. Oshima, Y. Yamada-Takamura, Y. Takahashi, S. Okada, T. Kato, and Y. Miyata, Nanoscrolls of Janus Monolayer Transition Metal Dichalcogenides, ACS Nano, **18**, 2772–2781 (2024).

[11] R. Kesarwani, M. Veverka, M. Žáček, V. Varade, L. Fekete, M. Kalbac, and J. Vejpravova, Unveiling the Giant Polarisation Ratio of Chiral TMD Nanorolligami: A New Platform for Polarization-Selective Optoelectronics, Nanoscale Horiz., **10**, 2972–2983 (2025).

[12] V. Varade, G. Haider, M. Kalbac, and J. Vejpravova, Sulfur Isotope Engineering in Heterostructures of Transition Metal Dichalcogenides, Nanoscale Adv., **7**, 1276–1286 (2025).

HYDROPHOBIC ZNFE2O4 MAGNETIC NANOPARTICLES WITH WELL-DEFINED SUPERBALL MORPHOLOGY AND ROOM-TEMPERATURE SUPERPARAMAGNETISM

DOI: 10.66951/PHIO6007; https://doi.org/10.66951/PHIO6007

Štefan Hricov, stefan.hricov@matfyz.cuni.cz
Department of Condensed Matter Physics, Faculty of Mathematics and Physics, Ke Karlovu 5, 121 16 Prague, Czechia

Dominika Zákutná, zakutnad@ill.fr
Institut Laue-Langevin - The European Neutron Source, 71 avenue des Martyrs, 38042 Grenoble, France

Jana Vejpravová, jana.vejpravova@matfyz.cuni.cz
Department of Condensed Matter Physics, Faculty of Mathematics and Physics, Ke Karlovu 5, 121 16 Prague, Czechia

Veronika Gajdošová, gajdosova@imc.cas.cz
Department of Polymer Morphology, Institute of Macromolecular Chemistry CAS, Heyrovského nám. 2, 162 00 Prague, Czechia

Abstract

For fundamental and applicative research, narrowly size-distributed magnetic nanoparticles are essential for drawing reliable correlations between structure and properties. Here, we report a robust synthesis protocol for $ZnFe_2O_4$ magnetic nanoparticles based on the thermal decomposition of metal-organic salts in the presence of oleic acid as a surfactant, performed in a high-boiling-point solvent. The morphological quality and size distribution of resulting nanoparticles were assessed by transmission electron microscopy and image analysis. Complementary characterization by powder X-ray diffraction and DC magnetometry provided insight into their structural and magnetic properties.

1 Introduction

Size-related effects provide a key access window into novel properties of materials, often contrasting with their bulk counterparts. In this context, the advent of magnetic nanoparticles (MNPs) research unravelled unprecedented applicative potential of this particular class of materials. MNPs are already in use or proposed to be implemented in hyperthermia cancer treatment[1,2], bio-imaging[3,4], spintronics[5] or catalysis[6]. Particularly, thanks to their excellent chemical stability, the ferrites are the subject of a sustained research interest over the years[7,8]. While the illustrious magnetite nanoparticles have received noticeable attention, due to their magnetic properties[9] and excellent biocompability[10], for an appropriate material selection designated for commercial use, a broad spectrum of deeply studied entries must be available. Therefore, among the comparatively underinvestigated ferrite MNPs are, for example, the $ZnFe_2O_4$ MNPs. In its bulk form, $ZnFe_2O_4$ possesses normal spinel structure and antiferromagnetic ordering below the Néel temperature ($T_N \approx 10$ K)[11]. However, as MNPs, $ZnFe_2O_4$ exhibits either ferrimagnetic or superparamagnetic behavior, depending on a given temperature regime[12]. To obtain $ZnFe_2O_4$ MNPs, various synthesis procedures were employed, such as co-precipitation[13] or synthesis under solvothermal conditions[14].

For adequate properties evaluation, it is essential to be able to fabricate $ZnFe_2O_4$ MNPs with narrow size distribution and well-defined morphology. To achieve this goal, we synthesize $ZnFe_2O_4$ via

thermal decomposition using high boiling point solvent. Morphological evaluation of resulting products was carried out using transmission electron microscopy (TEM), accompanied by respective image analysis with reconstructed size distribution. Moreover, to confirm presence of $ZnFe_2O_4$ phase, powder X-ray diffraction (PXRD) was performed. The diffraction pattern was analyzed using full-profile Rietveld refinement. Information about the sample's texture was further retrieved by employing spherical harmonics within the full-profile analysis. As for magnetic properties, the DC magnetometry was utilized resulting in ZFC-FC and several isothermal hysteresis loops.

2 Experimental

2.1 Synthesis of $ZnFe_2O_4$ nanoparticles

Iron(III) acetylacetonate (97%), zinc(II) acetylacetonate (99.995%), oleic acid (90%) and 1-octadecene (90%) dibenzylether (98%) were purchased from Sigma Aldrich, acetone (99.5%) and ethylacetate (≥ 99.5%) from VWR and finally ethanol (98%) from Penta Chemicals. $ZnFe_2O_4$ MNPs were prepared via thermal decomposition of organic metal salts. At first, 1.26 mmol of $Zn(acac)_2$ and

2.56 mmol of $Fe(acac)_3$ was weighed into a 50mL three-neck round bottom flask, followed by addition of 15.6 mmol of oleic acid (OA). Subsequently, 5 mL of 1-octadecene and dibenzylether was added and the reaction mixture was left to dissolve at 60 °C for 15 min under flowing N_2. The flask was placed into the heating mantle, and heating profile was started – first, the reaction was heated up to 290 °C at a heating rate of 7.67 °C/min. Subsequently, a 1-hour plateau was maintained at this temperature. After the reaction ended, the 50mL three-neck round-bottom flask was removed from the heating mantle and allowed to cool down under ambient conditions. For the purpose of purification, the whole volume of reaction mixture was transferred into a 50mL Falcon® tube. Residual product remaining inside the round-bottom flask was washed out using *approx.* 5 mL of toluene. Furthermore, *approx.* 20 ml of reaction mixture were evenly divided in total among four 50mL Falcon® test tubes. Then, into each one of them, 10 mL of iPrOH, 8 mL of EtOAc and 2 mL of EtOH were added. Solvent addition was followed by centrifugation at 7830 RPM (6511 g) for 30 min. The resulting dark-colored opaque supernatant was discarded, and pellets were redispersed in 5 mL of toluene. Eventually, 5 mL of iPrOH, 4 mL of EtOAc and 1 mL of EtOH were added to the redispersed MNPs and centrifuged at 7830 RPM (6511 g) for 10 min. Transparent, brownish supernatant was discarded, MNPs were redispersed in 5 mL of toluene and collected.

3 Results and Discussion

3.1 Transmission electron microscopy

Morphological evaluation was performed by transmission electron microscopy (TEM), utilizing a Tecnai G2 Spirit microscope from FEI operating at 120 kV. Bright-field micrographs (**Figure 1A, 1B)** reveal a well-defined superball morphology with a high degree of the shape uniformity. To determine the size distribution of MNPs system, image analysis was performed on the micrographs and the resulting histogram, (**Figure 1C)**, was fitted with a log-normal function, yielding a mean particle diameter of d_{TEM} = 18.32(6) nm and a polydispersity of 8.2(3) %, indicating narrowly distributed, monodisperse system.

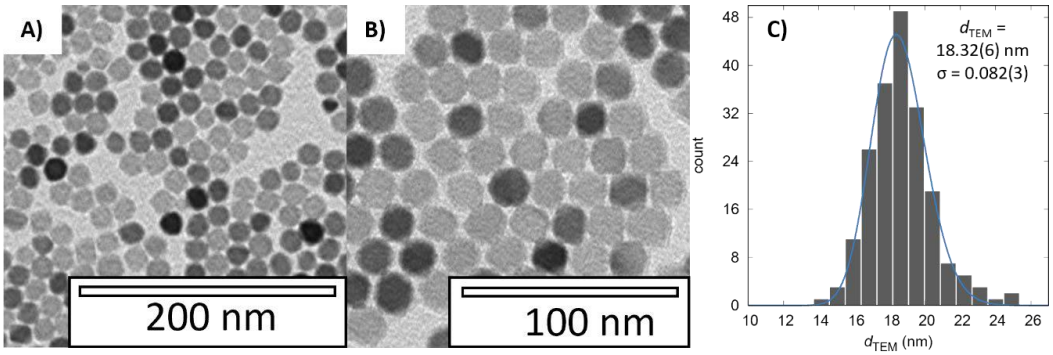


Figure 1. A) TEM-BF micrograph of ZnFe2O4 MNPs Detailed look on MNPs is on a zoomed micrograph, B). C) size distribution with fitted log-normal function, obtained from the image analysis of TEM BF micrographs.

3.2 Powder X-ray diffraction

Phase composition was confirmed by PXRD using a Panalytical X'pert Pro diffractometer equipped with Cu K_α radiation. Observed diffraction pattern was analyzed by full-profile Rietveld refinement in WinPLOTR (FullProf suite [15,16]), incorporating SPHR texture refinement to extract directional crystallite size parameters. Contributions from instrumental broadening were accounted for by calculating instrumental resolution function, based on the LaB_6 diffraction pattern. The refined pattern (**Figure 2A)** confirms the spinel $ZnFe_2O_4$ phase with no detectable impurities. From the Lorentzian broadening, an apparent crystallite size of d_{PXRD} = 14.6(7) nm was obtained, which is notably smaller than d_{TEM}. This discrepancy indicates that the coherently scattering domain does not extend to the full physical boundary of nanoparticles, consistent with the structural disorder in the near-surface layers, as commonly observed in nanoscale system. Independently, the crystallite shape reconstructed from the SPHR refinement (**Figure 2B**) is consistent with superball morphology identified by TEM, providing corroborating evidence for the morphological uniformity of the sample. To emphasize direction- dependent size parameters retrieved from the SPHR refinement, one may consider **(Figure 2C)** with illustrative directional indicators.

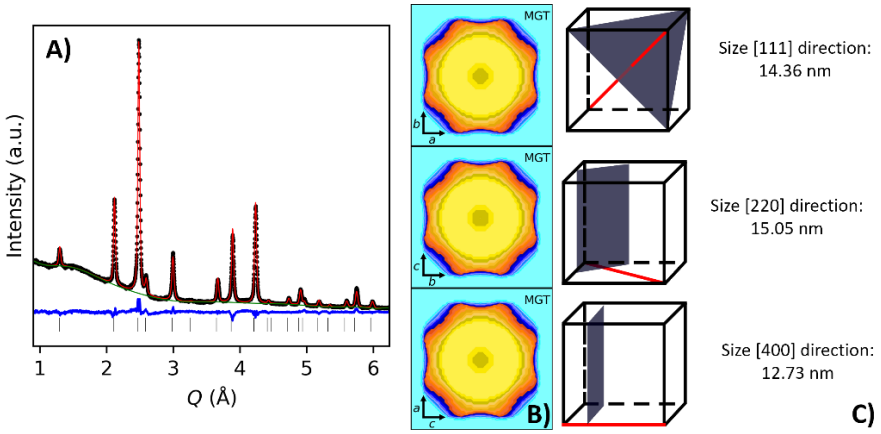


Figure 2. A) PXRD of MNPs with SPHR fit, where black dots represent observed intensity, red curve calculated pattern, green curve a background function (Chebyshev polynomials) and the blue curve is difference between calculated and observed intensity. Diffraction maxima of ZnFe2O4 phase are depicted as black vertical lines. B) Average crystallite shape is accompanying the diffraction pattern. C) Direction-dependent size parameters are shown alongside the corresponding schematic direction indicators.

3.3 Magnetic measurements

To prepare powder sample, the MNPs toluene dispersion was dried in a watch glass and homogenized in a mortar. A 7.7 mg aliquot was loaded into a Vibrating Sample Magnetometry (VSM) powder sample capsule, fixed with cyanoacrylate adhesive, and measured on the physical property measurement system (PPMS) from Quantum Design equipped with VSM module. The ZFC/FC magnetization curves, measured under an applied magnetic field of 10 mT are shown in **(Figure 3A).** The blocking temperature, T_B was estimated from the peak in the temperature derivative of the ZFC – FC magnetization difference **(Figure 3B)** yielding $T_B \approx 19$ K. A series of isothermal hysteresis loops recorded at selected temperatures, **(Figure 3D)**, clearly shows progressive increase in saturation magnetization upon cooling, consistent with enhanced spin alignment. Moreover, at 3 K and below T_B, the MNPs reside in the blocked state and exhibit a ferrimagnetic response, evidenced by a weak but finite coercivity of $\mu_0 H_c = 21$ mT. To probe for a potential exchange bias arising from pinned surface magnetic moments, the sample was field-cooled to 3 K under 7T applied field and a subsequent hysteresis loop was recorded **(Figure 3D)**. The FC hysteresis loop shows no horizontal shift, $\mu_0 H_c =$ 21 mT remaining identical to its zero-field-cooled counterpart, unambiguously ruling out exchange-bias contribution.

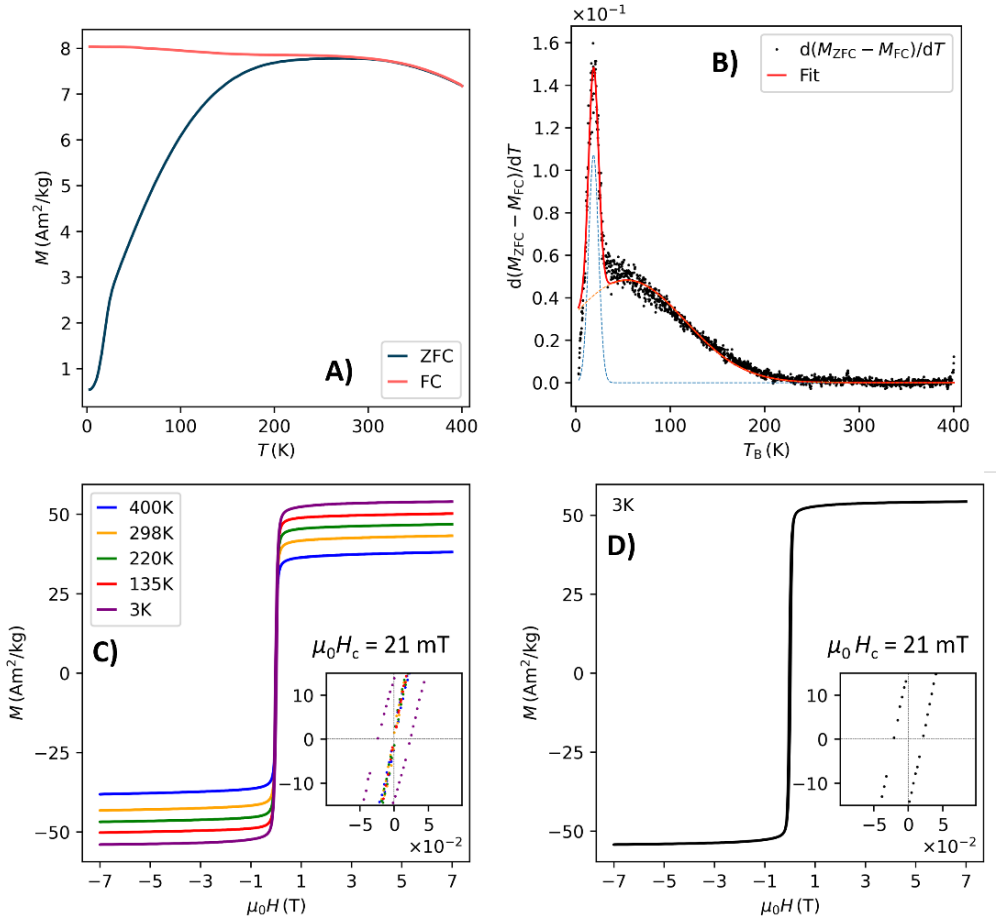


Figure 3. A) ZFC-FC temperature dependent magnetization measurement, B) temperature ZFC-FC magnetization difference derivative with estimated *T*B, C) series of isothermal hysteresis loops with zoomed inset for coercivity evaluation and D) FC-hysteresis (7 T cooling field, 3 K) with zoomed inset.

4 Summary

To fabricate monodisperse and morphologically well-developed superball $ZnFe_2O_4$ MNPs, the thermal decomposition of metal-organic salts in a high-boiling-point solvent was utilized. MNPs, with a size of 18.32(6) nm and polydispersity of 8.2(3) % were obtained. To confirm presence of $ZnFe_2O_4$ phase, the PXRD pattern was recorded and subsequently analyzed by full-profile analysis. Magnetic

characterization unveiled low $T_B \approx 19$ K together with minuscule $\mu_0 H_c = 21$ mT recorded at 3 K. Moreover, the FC-hysteresis disproves pinning of magnetic moments within the MNPs. Taken together, these results demonstrate that the synthesized $ZnFe_2O_4$ MNPs exhibit robust room-temperature superparamagnetic, defining property that makes this system attractive for biomedical and technological applications where a magnetically switchable, remanence-free response is required. Given the relative scarcity of well-characterized $ZnFe_2O_4$ systems in the literature compared to magnetite, this work provides a reproducible synthetic benchmark and a complete structural–magnetic property profile against which future studies can be referenced.

5 Acknowledgement

This work has been funded by a grant from the Programme Johannes Amos Comenius under the Ministry of Education, Youth and Sports of the Czech Republic CZ.02.01.01/00/22_008/0004558 Advanced MUltiscaLe materials for key Enabling Technologies.

6 References

[1] M. Lin, J. Huang, and M. Sha, Recent Advances in Nanosized Mn-Zn Ferrite Magnetic Fluid Hyperthermia for Cancer Treatment, Journal of Nanoscience and Nanotechnology **14**, 792 (2014).

[2] E. Mazario, N. Menéndez, P. Herrasti, M. Cañete, V. Connord, and J. Carrey, Magnetic Hy- perthermia Properties of Electrosynthesized Cobalt Ferrite Nanoparticles, American Chemical Society **117**, 11405 (2013).

[3] J. Estelrich, M. J. Sánchez-Martín, and M. A. Busquets, Nanoparticles in magnetic resonance imaging: from simple to dual contrast agents, International Journal of Nanomedicine **10**, 1727 (2015).

[4] K.-S. Kim, J.-H. Han, J.-H. Park, H.-K. Kim, S. H. Choi, G. R. Kim, H. Song, H. J. An, D. K. Han, W. Park, and K.-S. Park, Multifunctional nanoparticles for genetic engineering and bioimaging of natural killer (NK) cell therapeutics, Biomaterials **221**, 119418 (2019).

[5] Q. K. Ong, X.-M. Lin, and A. Wei, Role of Frozen Spins in the Exchange Anisotropy of Core-Shell Fe@Fe3O4 Nanoparticles, J. Phys. Chem. C **115**, 2665 (2011).

[6] L. M. Rossi, N. J. S. Costa, F. P. Silva, and R. Wojcieszak, Magnetic nanomaterials in catalysis: advanced catalysts for magnetic separation and beyond, Green Chem., **16**, 2906–2933 (2014).

[7] Y. Ichiyanagi, M. Kubota, S. Moritake, Y. Kanazawa, T. Yamada, and T. Uehashi, Magnetic properties of Mg-ferrite nanoparticles, J. Magn. Magn. Mat., **310**, 2378–2380 (2007).

[8] A. López-Ortega, E. Lottini, C. de J. Fernández, and C. Sangregorio, Exploring the Magnetic Properties of Cobalt-Ferrite Nanoparticles for the Development of a Rare-Earth-Free Permanent Magnet, Chem. Mater., **27**, 4048–4056 (2015).

[9] Y. Wei, B. Han, X. Hu, Y. Lin, X. Wang, and X. Deng, Synthesis of Fe3O4 Nanoparticles and their Magnetic Properties, Procedia Eng., **27**, 632–637 (2012).

[10] P. Figueiredo, K. Lintinen, A. Kiriazis, V. Hynninen, Z. Liu, T. Bauleth-Ramos, A. Rahikkala, A. Correia, T. Kohout, B. Sarmento, J. Yli-Kauhaluoma, J. Hirvonen, O. Ikkala, M. Kostiainen, and H. Santos, In vitro evaluation of biodegradable lignin-based nanoparticles for drug delivery and enhanced antiproliferation effect in cancer cells, Biomaterials, **121**, 97–108 (2017).

[11] J. Gass, H. Srikanth, N. Kislov, S. Srinivasan, and Y. Emirov, Magnetization and magnetocaloric effect in ball-milled zinc ferrite powder, J. Appl. Phys., **103**, 07B309 (2008).

[12] V. Blanco-Gutierrez, E. Climent-Pascual, M. Torralvo-Fernandez, R. Saez-Puche, and M. Fernandez-Diaz, Neutron diffraction study and superparamagnetic behavior of $ZnFe_2O_4$ nanoparticles obtained with different conditions, J. Solid State Chem., **184**, 1608–1613 (2011).

[13] R. Haghniaz, A. Rabbani, F. Vajhadin, T. Khan, R. Kousar, A. Khan, H. Montazerian, J. Iqbal, A. Libanori, H.J. Kim, and F. Wahid, Antibacterial and wound healing-promoting effects of zinc ferrite nanoparticles, J. Nanobiotechnology, **19**, 38 (2021).

[14] P. Lyu, Y. Hou, R. Wang, M. Ma, Y. Chen, Q. Xing, Y. Ma, S. Wang, Y. Wu, and W. Huang, Synthesis of $ZnFe_2O_4$@Mg-Al-SDBS LDH composites for regulating heat and fire safety properties of polyurea, Polym. Adv. Technol., **33**, 4290–4301 (2022).

[15] J. Rodríguez-Carvajal, Recent advances in magnetic structure determination by neutron powder diffraction., Physica B: Condensed Matter, **192**, 55-69 (1993).

[16] T. Roisnel, J. Rodríguez-Carvajal, WinPLOTR: a Windows tool for powder diffraction patterns analysis, Materials Science Forum, Proceedings of the Seventh European Powder Diffraction Conference (EPDIC 7), 118-123 (2000).

ION-BEAM ENGINEERING AS A PHYSICAL STRATEGY FOR ELECTROCHEMICAL MATERIALS DESIGN

DOI: 10.66951/GFAW9691; https://doi.org/10.66951/GFAW9691

E. Štěpanovská, stepanovska@ujf.cas.cz
Institute of Nuclear Physics of the Czech Academy of Sciences, Řež 292, 250 68 Husinec, Czech Republic; Department of Physics, Faculty of Science, J. E. Purkyně University, Pasteurova 3632/15, 400 96 Ústí nad Labem, Czech Republic

J. Novák; novak@ujf.cas.cz
Institute of Nuclear Physics of the Czech Academy of Sciences, Řež 292, 250 68 Husinec, Czech Republic; Department of Physics, Faculty of Science, J. E. Purkyně University, Pasteurova 3632/15, 400 96 Ústí nad Labem, Czech Republic

P. Malinský, malinsky@ujf.cas.cz
Institute of Nuclear Physics of the Czech Academy of Sciences, Řež 292, 250 68 Husinec, Czech Republic; Department of Physics, Faculty of Science, J. E. Purkyně University, Pasteurova 3632/15, 400 96 Ústí nad Labem, Czech Republic

R. Mikšová, miksova@ujf.cas.cz
Institute of Nuclear Physics of the Czech Academy of Sciences, Řež 292, 250 68 Husinec, Czech Republic

G. Ceccio, ceccio@ujf.cas.cz
Institute of Nuclear Physics of the Czech Academy of Sciences, Řež 292, 250 68 Husinec, Czech Republic

B. Wu, Bing1.Wu@vscht.cz
University of Chemistry and Technology, Prague, Technická 5, 166 28 Prague 6, Czech Republic

V. Mazánek, Vlastimil.Mazanek@vscht.cz
University of Chemistry and Technology, Prague, Technická 5, 166 28 Prague 6, Czech Republic

M. Kormunda, martin.kormunda@ujep.cz
Department of Physics, Faculty of Science, J. E. Purkyně University, Pasteurova 3632/15, 400 96 Ústí nad Labem, Czech Republic

L. Vrtoch, lubos.vrtoch@ujep.cz
Department of Physics, Faculty of Science, J. E. Purkyně University, Pasteurova 3632/15, 400 96 Ústí nad Labem, Czech Republic

A. Macková, mackova@ujf.cas.cz
Institute of Nuclear Physics of the Czech Academy of Sciences, Řež 292, 250 68 Husinec, Czech Republic; Department of Physics, Faculty of Science, J. E. Purkyně University, Pasteurova 3632/15, 400 96 Ústí nad Labem, Czech Republic

Abstract

Ion-beam modification represents a versatile physical strategy for tailoring the electrochemical properties of materials without the need for conventional chemical functionalization. This work demonstrates the potential of multi-energy Cu and Ag ion implantation for engineering two distinct

classes of energy storage materials: polymer interfaces and multilayer graphene. A combination of ion-beam simulations, structural and chemical characterization, theoretical calculations, and electrochemical analyses revealed that implantation induces controlled defect formation, local bond rearrangement, and stabilization of implanted atoms, resulting in modified electrochemical behavior. In polymer materials, these changes enhanced interfacial polarization while preserving the predominantly insulating character of the matrix. In multilayer graphene, ion implantation introduced controlled structural modifications, affected the interlayer arrangement, and tuned the electrochemical response of the anode material. The results demonstrate that multi-energy ion implantation provides a transferable physical approach for engineering electrochemical materials and highlights its potential as an alternative to conventional chemical modification strategies for future energy storage applications.

Introduction

The development of advanced materials for electrochemical and energy storage applications is commonly based on chemical functionalization, which enables tuning of structural, electronic, and interfacial properties through the introduction of new functional groups or chemically active species [1]. Although highly effective, these approaches are often material-specific, require multistep synthesis procedures, and may be difficult to transfer between different classes of materials [1].

Ion-beam modification offers an alternative physical strategy for tailoring material properties without altering the overall architecture of the material. During ion implantation, energetic ions transfer energy to the target through electronic excitation and nuclear collisions, inducing controlled defect formation, bond rearrangement, local structural modifications, and stabilization of implanted atoms [2]. Unlike conventional chemical methods, these processes can be achieved using the same implantation approach across chemically distinct materials while preserving their macroscopic integrity [2,3].

In this work, the potential of multi-energy Cu and Ag ion implantation is demonstrated using two representative classes of electrochemical materials: polymer interfaces and multilayer graphene. Although these materials differ fundamentally in their chemical composition, structure, and function, both benefit from controlled ion-beam-induced modification. In polymers, implantation promotes the formation of electrochemically active interfacial regions with enhanced polarization behavior, whereas in graphene it enables controlled structural tuning of the electrode architecture for lithium-ion storage [3,4]. The presented results demonstrate that multi-energy ion implantation represents a versatile physical strategy for engineering electrochemical materials and highlights its potential as an alternative to conventional chemical modification for future energy storage technologies.

4 Experimental

Polyimide (PI), poly (methyl methacrylate) (PMMA), and cyclic olefin copolymer (COC) films (thickness 50 μm) were obtained from Goodfellow (UK) and Polyplastics Co. (Japan). A commercially available graphene sheet (35 μm thick, 10 × 10 cm) supplied by Nanografi (Turkey) was used as a representative multilayer graphene material. Cu^+ and Ag^+ ions were implanted into all materials using a Tandetron 4130 MC accelerator. Multi-energy implantation was performed sequentially at 2.8, 2.0, and 1.2 MeV with ion fluences of 1×10^{12}, 1×10^{13}, and 1×10^{14} cm^{-2}. The beam current density was maintained at 15–45 nA cm^{-2} to minimize beam-induced heating and preserve the integrity of the implanted materials.

The implantation process was designed to produce an extended subsurface modified region by overlapping the ion ranges corresponding to the three implantation energies. Structural, chemical, and electrochemical changes induced by ion implantation were subsequently evaluated using

complementary characterization techniques, including SRIM simulations, DFT calculations, RBS/ERDA, FTIR, XPS, Raman spectroscopy, X-ray diffraction (XRD), electrochemical impedance spectroscopy (EIS), galvanostatic charge–discharge measurements, and electrical characterization, depending on the investigated material.

5 Results and Discussion

5.1 A Common Physical Strategy for Materials Engineering

The first step of this study was to verify whether the same ion-beam approach could be applied to chemically and structurally different electrochemical materials. Stopping and Range of Ions in Matter (SRIM) simulations were employed to model the ion–solid interactions and predict implantation profiles. As shown in **Figure 1.**, SRIM simulations performed for PI implanted with Cu and Ag ions indicated that sequential implantation at 2.8, 2.0, and 1.2 MeV produced overlapping implantation profiles, resulting in an extended subsurface modified region rather than a modification confined to the immediate surface. The projected ion ranges depended on the implanted ion species and the target material, while the combination of three implantation energies enabled the deposited energy and implanted atoms to be distributed over a broader depth range.

Unlike conventional chemical functionalization, which is generally limited to surface-accessible regions, multi-energy ion implantation provides a physical strategy for tailoring materials through controlled subsurface modification. During ion implantation, energy is transferred through electronic excitation and nuclear collisions, leading to gradual structural rearrangement, defect formation, and local physicochemical activation of the material [2,3]. To complement the SRIM depth profiles, DFT calculations were used to clarify how implantation-induced dehydrogenation can create active sites capable of stabilizing Cu and Ag atoms in the modified polymer structure, as illustrated in **Figure 2**. Together, the SRIM and DFT results show that the same implantation strategy can be used not only to control the depth of modification, but also to support the chemical stabilization of implanted species in electrochemically relevant materials.

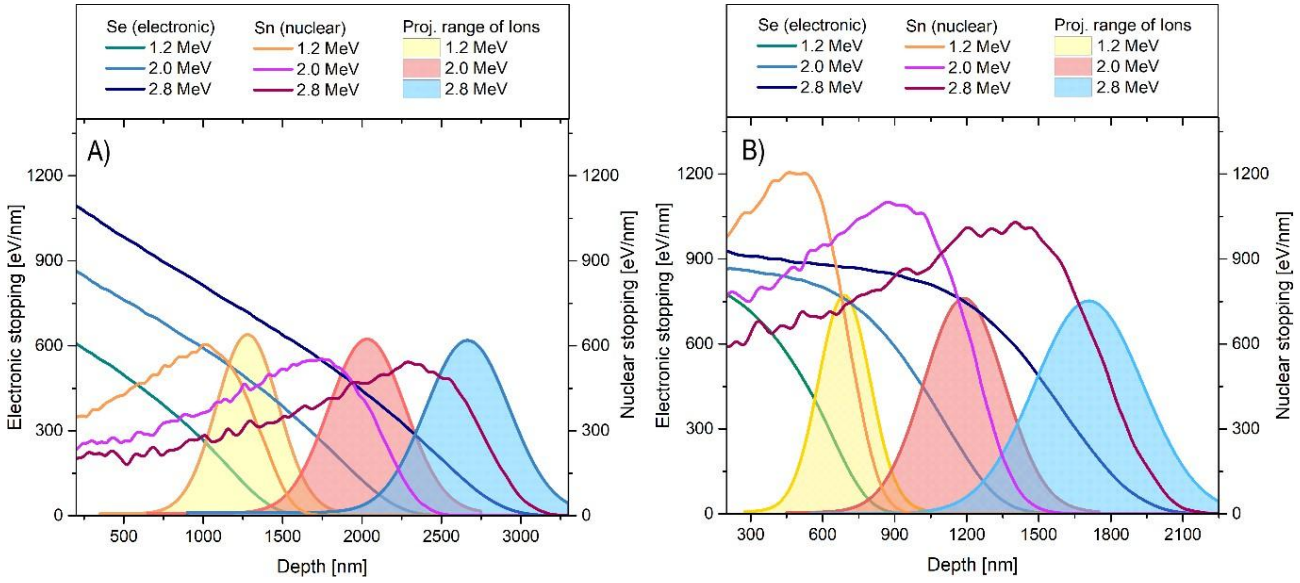


Figure 1. SRIM simulation of multi-energy ion implantation into polyimide (PI): implantation profiles for Cu ions (A) and Ag ions (B). The simulations demonstrate the formation of overlapping ion distributions produced by sequential implantation at different energies, leading to an extended subsurface modified region.

5.2 Engineering the Material–Electrolyte Interface

Although the investigated materials differ in their structure and function, both are relevant for energy storage applications because their electrochemical behavior is strongly influenced by the material–electrolyte interface [7]. Polymer materials can act as functional interfacial, protective, dielectric, or polarization-active layers, where the key requirement is not high electronic conductivity, but controlled interaction with ions and electrolyte species [7,8]. In contrast, multilayer graphene represents a conductive carbon-based electrode material, where structural order, defect density, surface chemistry, and interlayer spacing directly affect lithium-ion storage and transport [4,6]. In both systems, multi-energy ion implantation modifies precisely the region that is essential for electrochemical performance. The implanted ions do not affect only the outermost surface but create an extended near surface and subsurface region with altered physicochemical properties. In polymers, this modification leads to defect formation, dehydrogenation, local oxidation, and stabilization of implanted metal atoms, which together contribute to enhanced interfacial polarization. In multilayer graphene, implantation introduces controlled disorder into the graphitic structure, increases the interlayer spacing as confirmed by XRD, and changes the surface chemistry of the electrode material. This concept is illustrated in **Figure 2.** for the COC polymer system, showing the pristine COC structure and the corresponding changes in electrochemical response after ion implantation. Although this example focuses on COC, it illustrates the broader mechanism observed in this work: ion-beam-induced defects and chemical rearrangements can transform an originally passive or weakly active polymer interface into a more electrochemically responsive region [2,3]. Therefore, the role of ion implantation is not limited to introducing radiation damage. Instead, controlled defect formation can be used as a functional tool for designing material–electrolyte interfaces [5,7]. This makes multi-energy ion implantation a versatile physical strategy for tailoring electrochemical materials across different material classes, from polymer-based interfacial layers to graphene-based electrodes [2,5].

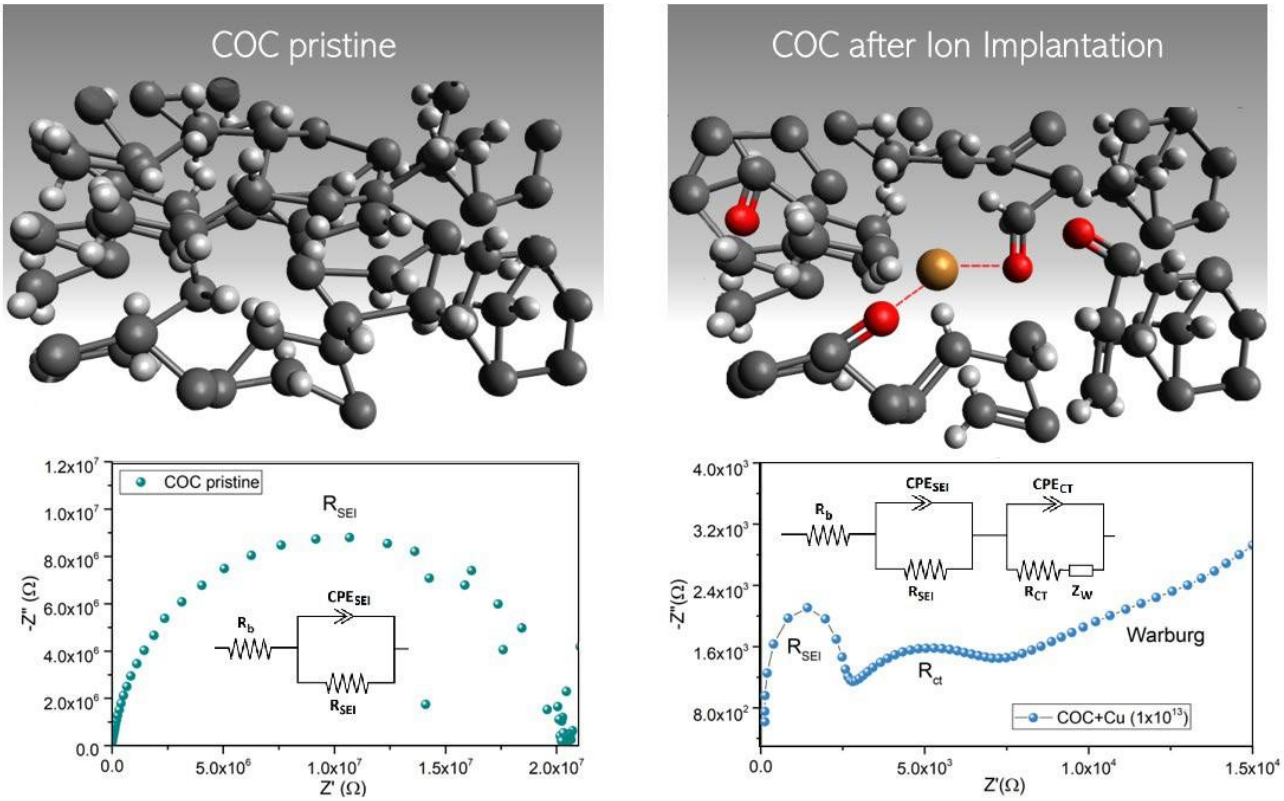


Figure 2. Schematic representation of the COC polymer system and its electrochemical modification after ion implantation. The figure shows the pristine COC structure and illustrates how implantation-induced defects and chemical rearrangements alter the electrochemical response of the polymer interface.

Conclusion

This work demonstrates that multi-energy Cu and Ag ion implantation can be used as a transferable physical strategy for tailoring electrochemical materials with fundamentally different structures and functions. Sequential implantation energies produced an extended near-surface and subsurface modified region, enabling controlled defect formation, local bond rearrangement, and stabilization of implanted metal atoms. In polymer materials, these changes promoted electrochemically responsive interfacial regions with enhanced polarization behavior, while in multilayer graphene, ion implantation introduced controlled structural disorder, increased the interlayer spacing confirmed by XRD, and modified the electrochemical response of the anode material. Overall, the comparison of polymer interfaces and multilayer graphene highlights that the same physical principle can be applied across distinct material classes, offering a versatile route for the design of future energy storage materials without relying solely on conventional chemical functionalization.

5 Acknowledgement

The instrumental development has been carried out at the CANAM (Centre of Accelerators and Nuclear Analytical Methods) infrastructure LM2015056. The scientific results were obtained with the support of the GACR Project No. 22-10536S and University of J. E. Purkyně project UJEP-SGS-2023-53-007-2. The authors acknowledge the assistance provided by the Advanced Multiscale Materials for Key Enabling Technologies project, supported by the Ministry of Education, Youth and Sports of the Czech Republic, Project No. CZ.02.01.01/00/22_008/0004558, co-funded by the European Union.

6 References

[1] Baumann, A. E., Burns, D. A., Liu, B., & Thoi, V. S. Metal-organic framework functionalization and design strategies for advanced electrochemical energy storage devices. Communications Chemistry, 2019, 2, 86. DOI: 10.1038/s42004-019-0184-6.

[2] Zhang, Y., & Weber, W. J. Ion irradiation and modification: The role of coupled electronic and nuclear energy dissipation and subsequent nonequilibrium processes in materials. Applied Physics Reviews, 2020, 7, 041307. DOI: 10.1063/5.0027462.

[3] Akhtar, A. N., Murtaza, G., Shafique, M. A., & Haidyrah, A. S. Effect of Cu ions implantation on structural, electronic, optical and dielectric properties of polymethyl methacrylate (PMMA). Polymers, 2021, 13, 973. DOI: 10.3390/polym13060973.

[4] Ji, K., Han, J., Hirata, A., Fujita, T., Shen, Y., Ning, S., Liu, P., Kashani, H., Tian, Y., Ito, Y., Fujita, J.-i., & Oyama, Y. Lithium intercalation into bilayer graphene. Nature Communications, 2019, 10, 275. DOI: 10.1038/s41467-018-07942-z.

[5] Zhao, Z., Chen, H., Zhang, W., Yi, S., Chen, H., Su, Z., Niu, B., Zhang, Y., & Long, D. Defect engineering in carbon materials for electrochemical energy storage and catalytic conversion. Materials Advances, 2023, 4, 1241–1264. DOI: 10.1039/D2MA01009G.

[6] Lee, J., Kim, C., Cheong, J. Y., & Kim, I.-D. An angstrom-level d-spacing control of graphite oxide using organofillers for high-rate lithium storage. Chem, 2022, 8, 2393–2409. DOI: 10.1016/j.chempr.2022.06.020.

[7] Chen, Z., Li, M., Qi, S., & Du, L. Enhanced interfacial contact and lithium-ion transport in ionic liquid polymer electrolyte via in-situ electrolyte-cathode integration. Molecules, 2025, 30, 395. DOI: 10.3390/molecules30020395.

[8] Raghu, S., Devendrappa, H., Ganesh, S., & Matteppanavar, S. Modification of PEO-based polymer electrolytes by electron beam irradiation for energy storage applications. Colloid and Polymer Science, 2022, 300, 153–164. DOI: 10.1007/s00289-021-03977-3.

ACTIVATED BORANE MATERIALS FOR HETEROGENEOUS CATALYTIC DEHALOGENATION

DOI: 10.66951/PNOC2840, https://doi.org/10.66951/PNOC2840

Martin Lamač,* martin.lamac@heu.cas.cz
Heyrovský Institute of the CAS, Czechia

Béla Urbán
Heyrovský Institute of the CAS, Czechia

Abhishek Udnoor
Institute of Inorganic Chemistry of the CAS, Czechia

Michal Horáček
Heyrovský Institute of the CAS, Czechia

Jan Demel
Institute of Inorganic Chemistry of the CAS, Czechia

Abstract

In this contribution, we review our catalytic studies of activated borane (**ActB**) materials with different Lewis acid strength of their active centers utilized as heterogeneous catalysts for reductive dehalogenation of sp^3 C-X bonds using triethylsilane as the reductant. The increased Lewis acidity of the materials enabled lowering the reaction temperatures and expansion of the substrate scope even on perfluorinated pollutants.

Introduction

Reactions catalyzed by acidic catalysts play a significant role in chemistry, including a number of industrial processes. Heterogeneous catalysis predominates in these cases due to the many advantages it offers. On the other hand, strong molecular Lewis acids, such as borane derivatives, particularly $B(C_6F_5)_3$ (BCF),[1] have been used in a number of reactions as homogeneous catalysts. Our collaborating group recently introduced a new class of materials named after activated carbon – "activated borane" (**ActB**) – due to a similar nature of these porous amorphous polymers. **ActB**s are prepared by co-thermolysis of decaborane(14) (*nido*-$B_{10}H_{14}$) and various hydrocarbons.[2] **ActB**s possess relatively strong Lewis acid centers, likely corresponding to tricoordinated boron atoms in the material's structure. Thanks to these properties, they can be used as heterogeneous catalysts for reactions similar to those where its molecular analog BCF is employed. We have previously studied catalytic properies of **ActB**s formed from toluene, cyclohexane and *n*-hexane in reductive deoxygenation/hydrosilylation reactions of carbonyl substrates and also in dehydration of ethanol to ethylene.[3] As a next step, we studied reductive dehalogenation of aliphatic organohalides using triethylsilane as a method of catalytic removal/conversion of harmful halogenated substances.[4]

Preparation of ActB and its postsynthetic modification by bromine

The standard **ActB-Tol** material was prepared by heating a solution of *nido*-$B_{10}H_{14}$ in dry toluene to 250 °C in a stainless-steel autoclave for 24 h (Fig. 1). After this time, a black-brown powder appeared, which was Soxhlet-extracted with toluene and dried under vacuum. **ActB-Tol** was subsequently treated with excess of neat bromine under argon atmosphere for 24 h and the obtained solid was washed with toluene and dried under vacuum to afford the brominated material **ActB-Br**. Analyses of the new material revealed that the porous character was retained during the bromination, although the BET specific surface area decreased from 827 to 391 m^2g^{-1}. This was accompanied by changes in textural properties observable by SEM (insets in Fig. 1).

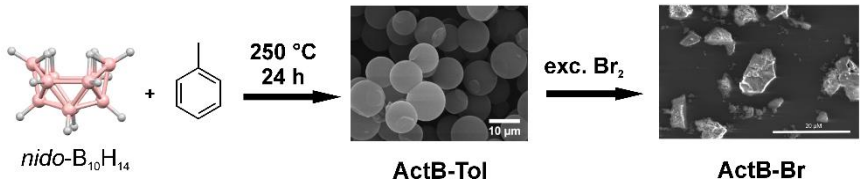


Figure 1. Preparation of ActB-Tol and its post-synthetic modification by bromine to give ActB-Br. SEM images are displayed for both materials obtained.
Gutmann-Beckett evaluation of Lewis acid strength of the boron active centres in the material revealed an increase (cf. ^{31}P chemical shift of the TEPO probe was 70.5 ppm for **ActB-Tol** and 73.0 ppm for **ActB-Br**).[5]

Catalytic dehalogenation

The proposed mechanism for the Lewis acid-catalysed reductive dehalogenation is depicted in Fig. 2. Activation of the Si-H bond in the silane is accompanied by the formation of carbocation by abstraction of the halogen atom from the substrate.

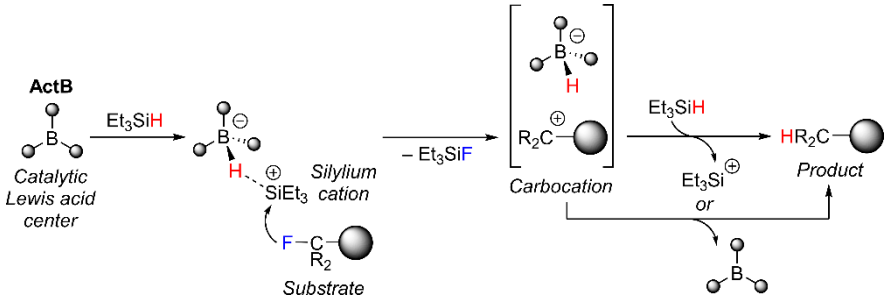


Figure 2. Proposed mechanism of the reductive dehalogenation (defluorination) using silane reductant catalysed by boron Lewis acid.

Reaction of α,α,α-trifluorotoluene with Et_3SiH was chosen as a model process. While the parent **ActB-Tol** gave 56% conversion of C–F bonds to Si–F bonds at 140 °C, **ActB-Br** reached complete C–F conversion already at 60 ◦C within 1 h, as confirmed by ^{19}F NMR, at the same substrate-to-catalyst ratio (Fig. 3).[5] The original material **ActB-Tol** was evaluated also with simple linear or cyclic aliphatic fluoro- and chloro-derivatives, while it proved sufficiently active at higher temperatures achieved conveniently by microwave heating (Fig. 3).[4] On the other hand, the more active ActB-Br has been screened for catalytic degradation of various fluorinated molecules, including the perfluorinated ones, which constitute some of the notorious persistent pollutants – such as the GenX precursor **11** (Fig. 4).[5]

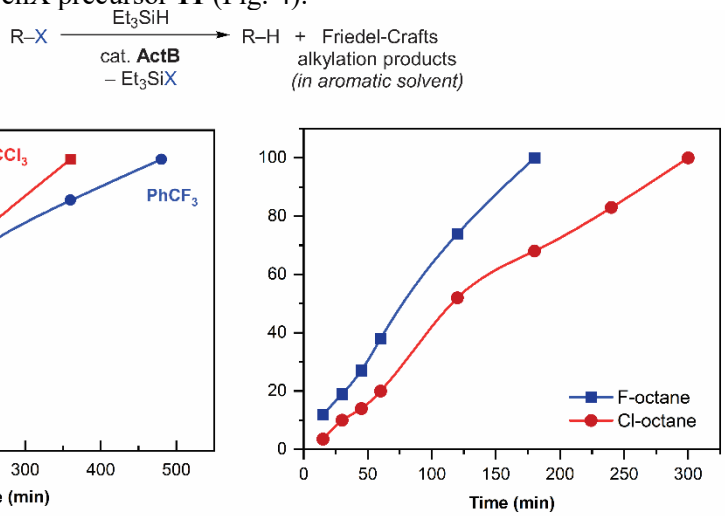


Figure 3. Selected catalytic dehalogenations using Et_3SiH catalysed by **ActB-Tol** – kinetic profiles at 140 °C using 20 mg of **ActB-Tol** per 1 mmol substrate.

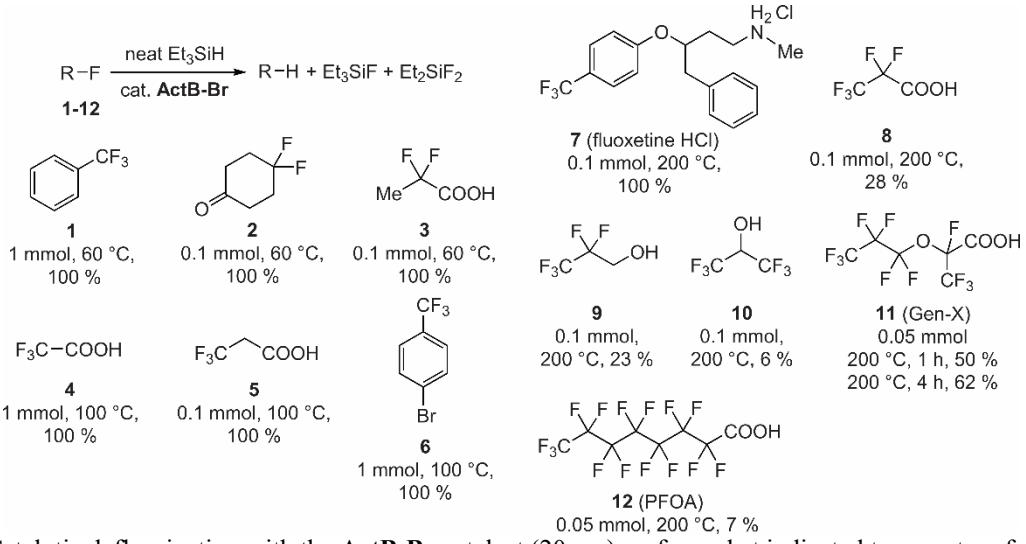


Figure 4. Catalytic defluorination with the **ActB-Br** catalyst (20 mg) performed at indicated temperature for 1 h in neat Et_3SiH (2 mL) as a solvent.

Notably, TON of 4098 was achieved for $PhCF_3$ and 156 for the GenX precursor **11**. The catalyst could be re-used by feeding new batches of the substrate (6 consecutive runs without observable loss of activity).

Conclusions

We demonstrated that bromination of an amorphous polymer based on borane clusters, **ActB**, is an effective strategy to enhance its Lewis acidity, leading to a marked improvement in catalytic performance in defluorination reactions. The increased Lewis acidity enabled lowering the reaction temperatures and expansion of the substrate scope even on perfluorinated pollutants.

Acknowledgement

This work has been funded by a grant from the Programme Johannes Amos Comenius under the Ministry of Education, Youth and Sports of the Czech Republic CZ.02.01.01/00/22_008/0004558 Advanced MUltiscaLe materials for key EnablingTechnologies.

Financial support by the Czech Science Foundation (grant no. 23-05818S) is acknowledged.

References

[1] (a) Piers, W. E.; Chivers, T. *Chem. Soc. Rev.* **1997**, *26*, 345–354; (b) Lawson, J.R.; Melen, R. L. *Inorg. Chem.* **2017**, *56*, 8627–8643.

[2] Bůžek, D.; Škoch, K.; Ondrušová, S.; Kloda, M.; Bavol, D.; Mahun, A.; Kobera, L.; Lang, K.; Londesborough, M.G.S.; Demel, J. *Chem. Eur. J.* **2022**, *28*, e202201885.

[3] Lamač, M.; Urbán, B.; Horáček, M.; Bůžek, D.; Leonová, L.; Stýskalík, A.; Vykydalová, A.; Škoch, K.; Kloda, M.; Mahun, A.; Kobera, L.; Lang, K.; Londesborough, M.G.S.; Demel, J. *ACS Catal.* **2023**, *13*, 14614−14626.

[4] Udnoor, A.; Urbán, B.; Škoch, K.; Hynek, J.; Horáček, M.; Lamač, M.; Demel, J. *Catal. Sci. Technol.* **2024**, *14*, 4458–4465.

[5] Udnoor, A.; Urbán, B.; Horáček, M.; Škoch, K.; Hynek, J.; Kloda, M.; Lamač, M.; Demel, J. *Mol. Catal.* **2026**, *601*, 116149.

NEGOTIATING OPEN SCIENCE: SOCIOLOGICAL PERSPECTIVES FROM THE AMULET PROJECT

DOI: 10.66951/AVVO7024; https://doi.org/10.66951/AVVO7024

Michal Trčka, michal.trcka@jh-inst.cas.cz
Heyrovsky Institute of the CAS, the Czech Republic

Abstract

Open Science has become one of the defining transformations of contemporary research systems. While international policies increasingly promote openness, FAIR data, and public accessibility as key principles of scientific practice, their implementation remains shaped by disciplinary differences, institutional contexts, and everyday research practices. This paper presents a qualitative case study of Open Science implementation within the AMULET project. Drawing on perspectives from Science and Technology Studies (STS), it combines qualitative sociological inquiry with participatory approaches to examine how Open Science is negotiated in the Czech research environment. The findings reveal tensions between Open Science principles and their implementation, particularly regarding research data management, disciplinary diversity, institutional preparedness, the evolving role of data stewards, and the sustainability of Article Processing Charges (APCs). The participatory activities demonstrate how digital deliberation can broaden researcher engagement and inform science policy. The paper argues that Open Science should be understood not merely as a technical or regulatory transformation, but as a continuous process of negotiation among researchers, institutions, funding agencies, and policymakers. Its successful implementation therefore depends not only on appropriate infrastructures and institutional support but also on participatory governance that actively involves the research community in shaping future Open Science policies.

Keywords: Open Science; Science and Technology Studies; sociology of science; research data management; Deliberative Participation; science policy.

1 Introduction

Open Science has become one of the defining transformations of contemporary research systems. During the last decade, international organizations, funding agencies, and research institutions have increasingly promoted openness, transparency, FAIR data, and public accessibility as central principles of scientific practice [1–3]. Open access publishing, research data management, and digital research infrastructures are now regarded as essential components of modern research ecosystems. At the same time, an increasing number of studies have shown that the implementation of Open Science is not merely a technical or administrative process but also represents a profound transformation of scientific cultures, disciplinary practices, institutional arrangements, and relationships between science and society [4–7].

From the perspective of Science and Technology Studies (STS), scientific knowledge is produced through interactions among researchers, institutions, technologies, regulations, and broader social contexts [7,8]. Consequently, Open Science should not be understood as a straightforward implementation of predefined policy requirements but rather as a continuous process of negotiation among multiple actors operating at different levels of the research system. While international,

European and national initiatives define common objectives, their practical implementation varies considerably across scientific disciplines, institutions, and local research environments.

The Czech research system has experienced a particularly rapid expansion of Open Science requirements in recent years, driven by European policies, national funding programmes, and institutional strategies. Although these developments have accelerated the adoption of FAIR principles and strengthened research data management practices, they have also introduced new administrative requirements, uncertainties regarding disciplinary differences, and ongoing debates concerning sustainable models of Open Access publishing.

These challenges have become especially visible within large interdisciplinary research projects, where researchers from different scientific backgrounds encounter common Open Science requirements while working with diverse research practices, data types, and publishing cultures. Such projects therefore provide a valuable opportunity to investigate how Open Science is interpreted and negotiated in everyday research practice.

This paper presents a qualitative case study conducted within the AMULET (Advanced MUltiscaLe materials for key Enabling Technologies) project. The paper combines selected results of qualitative sociological inquiry with participatory methods, including a public hearing and an online deliberative platform, to demonstrate both individual experiences and collective reflections on Open Science implementation.

This paper argues that successful implementation depends not only on technological solutions or institutional preparedness but also on recognizing disciplinary diversity and creating opportunities for meaningful participation by the research community. The aim of this paper is therefore to examine how Open Science is negotiated in everyday research practice through a qualitative case study conducted within the AMULET project and to demonstrate how qualitative inquiry combined with digital deliberation can contribute to evidence-informed science policy.

2 Work Performed: Negotiating Open Science in Practice

2.1 Qualitative Sociological Inquiry

The empirical research presented in this paper was conducted within the AMULET (Advanced MUltiscaLe materials for key Enabling Technologies) project between December 2024 and June 2025 [8]. Adopting a qualitative sociological approach inspired by Science and Technology Studies (STS), the study explored how Open Science is experienced and negotiated by researchers and other actors involved in its implementation.

The empirical material consisted of 31 semi-structured interviews with researchers, data stewards, project managers, and other project participants from different scientific disciplines. The interviews were complemented by participant observation and field research. Rather than evaluating compliance with Open Science policies, the study identified recurring challenges and experiences associated with their implementation in everyday research. The findings subsequently informed a public hearing and an online deliberative platform involving the wider Czech research community.

2.2 Negotiating Open Science in Everyday Research Practice

The interviews revealed a recurring tension between the principles of Open Science and their implementation in everyday research. While respondents generally supported openness and transparency,

and responsible research data management, many criticized the growing administrative burden associated with funding requirements and standardized procedures.

Disciplinary diversity emerged as one of the strongest themes. Participants emphasized that common Open Science requirements often fail to reflect differences between research fields. Researchers working with experimental materials and specialized datasets argued that identical requirements cannot always be applied across disciplines. Several respondents also criticized the specific "Czech approach" to implementation, suggesting that some national requirements exceed European standards.

Research data management represented another key topic. Although FAIR principles were widely recognized as beneficial, respondents highlighted practical limitations regarding data sharing and reproducibility. In materials science, for example, datasets alone often cannot capture laboratory knowledge, experimental skills, and specific equipment configurations required to reproduce experiments.

The interviews also highlighted the evolving role of data stewards. Most respondents performed this role alongside their research activities, creating additional professional demands. At the same time, many viewed data stewardship as an emerging profession with the potential to strengthen institutional Open Science capacity.

Institutional preparedness proved to be another important factor. Organizations that had invested in research data management infrastructure and support services before Open Science requirements became mandatory appeared considerably better prepared to meet funding expectations.

Finally, criticism of Article Processing Charges (APCs) was among the most frequently discussed issues. Respondents questioned the long-term sustainability of APC-based publishing models and expressed concerns about unequal access to Open Access publishing, reflecting broader international debates on the economics of scholarly communication [9].

2.3 From Qualitative Research to Public Deliberation

The qualitative findings formed the basis for a broader participatory reflection on Open Science. To extend the discussion beyond individual interviews, the AMULET project organized the public hearing *Making Sense of Open Science*, bringing together researchers, librarians, research managers, policymakers, funding organizations, and other stakeholders [10].

The discussions confirmed many of the challenges identified during the interviews, including disciplinary differences, increasing administrative demands, and concerns regarding APC-based publishing. They also expanded the debate towards national Open Science policy, particularly the potential introduction of Secondary Publishing Rights (SPR) as a mechanism for improving public access to publicly funded research while reducing dependence on APC-funded publishing [11].

The public hearing therefore served not only as a dissemination activity but also as a participatory validation of the qualitative findings, demonstrating that many identified challenges are shared across the Czech research system.

2.4 Online Deliberation and Policy Implications

To further broaden participation, the AMULET project implemented the eDemOS online deliberative platform [12], inspired by participatory democracy tools used, for example, in Taiwan. The platform enabled researchers and other stakeholders to discuss Open Science, vote on individual statements, and formulate recommendations for its future implementation in the Czech Republic.

The discussion revealed broad consensus on several issues. Participants supported creating Open Access publishing conditions comparable to those in countries such as Germany, including stronger protection of authors' publishing rights through mechanisms such as Secondary Publishing Rights. At the same time, the analysis identified two distinct opinion groups. Open Data Optimists represented 69.4% of participants, while Open Data Pessimists (30.6%), consisting predominantly of researchers from the natural sciences and engineering, expressed greater skepticism towards mandatory data sharing and the value of Data Management Plans, which they often perceived as an administrative burden rather than a meaningful research tool [13].

The outcomes of the online deliberation were subsequently presented and shared with selected members the Ministry of Education, Youth and Sports and the Czech Research, Development and Innovation Council. Together with the qualitative interviews and the public hearing, the deliberative platform demonstrates how social science research can not only analyze Open Science implementation but also create space for dialogue and contribute evidence-based recommendations for science policy.

3 Conclusions

This paper examined Open Science implementation through a qualitative case study conducted within the AMULET project. Combining qualitative sociological inquiry with participatory approaches, it demonstrated how Open Science is interpreted and negotiated by researchers and other actors involved in its implementation. The findings show that Open Science is shaped not only by technical infrastructures and policy requirements but also by interactions among researchers, institutions, funding agencies, and policymakers. While respondents broadly supported the principles of Open Science, they identified recurring challenges related to administrative burden, disciplinary diversity, research data management, the evolving role of data stewards, institutional preparedness, and the long-term sustainability of Article Processing Charges (APCs).

The study further demonstrates that qualitative inquiry can be effectively complemented by deliberative methods. The public hearing and online deliberative platform enabled a broader research community to validate the identified challenges, formulate recommendations, and contribute to discussions on Open Science policy. Together, these findings suggest that successful Open Science implementation requires not only appropriate infrastructures and institutional support but also participatory governance that actively involves researchers in shaping future science policy. The author's future research will continue to explore the implementation of Open Science in the Czech research environment, with particular attention to sustainable publishing models, participatory digital tools, and the growing role of artificial intelligence in research data management.

4 Acknowledgement

This work has been funded by a grant from the Programme Johannes Amos Comenius under the Ministry of Education, Youth and Sports of the Czech Republic CZ.02.01.01/00/22_008/0004558 Advanced MUltiscaLe materials for key Enabling Technologies.

5 References

[1] UNESCO. *UNESCO Recommendation on Open Science*. Paris: UNESCO; 2021.

[2] European Commission. *Turning FAIR into Reality: Final Report and Action Plan from the European Commission Expert Group on FAIR Data*. Luxembourg: Publications Office of the European Union; 2018.

[3] European Commission. *A New European Research Area for Research and Innovation*. COM (2020) 628 final. Brussels: European Commission; 2020.

[4] Barczak G, Griffin A, Kahn KB. How open is innovation research? An empirical analysis of data sharing among innovation scholars. *Industry and Innovation*. 2022;29(2):186–218. doi:10.1080/13662716.2021.1967727.

[5] Lakomý M, Hlaváček P, Macháček V. Open science and the science–society relationship. *Society*. 2019;56(3):246–255. doi:10.1007/s12115-019-00361-w.

[6] Jasanoff S, editor. *States of Knowledge: The Co-production of Science and Social Order*. London: Routledge; 2004.

[7] Mirowski P. The future(s) of open science. *Social Studies of Science*. 2018;48(2):171–203. doi:10.1177/0306312718772086.

[8] Stöckelová T, Trčka M. Qualitative sociological research on Open Science implementation within the AMULET project. Unpublished research, 2025–2026.

[9] Haustein S, Mongeon P, Alperin JP, et al. Estimating global article processing charges paid to six publishers for open access between 2019 and 2023. *Quantitative Science Studies*. 2024.

[10] Trčka M, Stöckelová T, et al. Making Sense of Open Science: Report on Public Hearing. Zenodo; 2025. doi:10.5281/zenodo.17390295.

[11] Knowledge Rights 21. Secondary Publishing Rights: How Europe Can Accelerate Transition to Open Access. Available at: https://knowledgerights21.org/publishing-rights/ (accessed 7 July 2026).

[12] Trčka M, Žabka V. eDemOS Deliberative Platform – public demo version. 2026. Available at: https://msp-r.mti.tul.cz/users/zabkav/amulet-main/ (accessed 7 July 2026).

[13] Trčka M, Žabka V. eDemOS Deliberative Platform: Summary of Online Discussion on the Implementation of Open Science in the Czech Republic. Zenodo. 2025. doi:10.5281/zenodo.17596626.

PARTNERS OF THE AMULET PROJECT

Heyrovský Institute

CHARLES UNIVERSITY

ÚJF NUCLEAR PHYSICS INSTITUTE The Czech Academy of Sciences

ÚOCHB AV ČR IOCB PRAGUE

UNIVERZITA J. E. PURKYNĚ V ÚSTÍ NAD LABEM

FZU Institute of Physics of the Czech Academy of Sciences

UNIVERSITY OF CHEMISTRY AND TECHNOLOGY PRAGUE

ÚFE Institute of Photonics and Electronics The Czech Academy of Sciences

Co-funded by the European Union

Ministry of Education, Youth and Sports of the Czech Republic

AMULET



As of 1st July 2026, we use the NEW name

Heyrovský Institute of the CAS (HI)

New name, same ambitions and new logo.

Heyrovský Institute



www.heu.cas.cz



Co-funded by the European Union

Ministry of Education, Youth and Sports of the Czech Republic

AMULET